AD-A072 831 UTAH STATE UNIV LOGAN ELECTRO-DYNAMICS LAB F/G 4/1
STUDIES OF ATMOSPHERIC INFRARED EMISSIONS.(U)
JAN 78 D J BAKER F19628-73-C-0048

UNCLASSIFIED AFGL-TR-78-0251 NL

1 OF 1
AD A072831

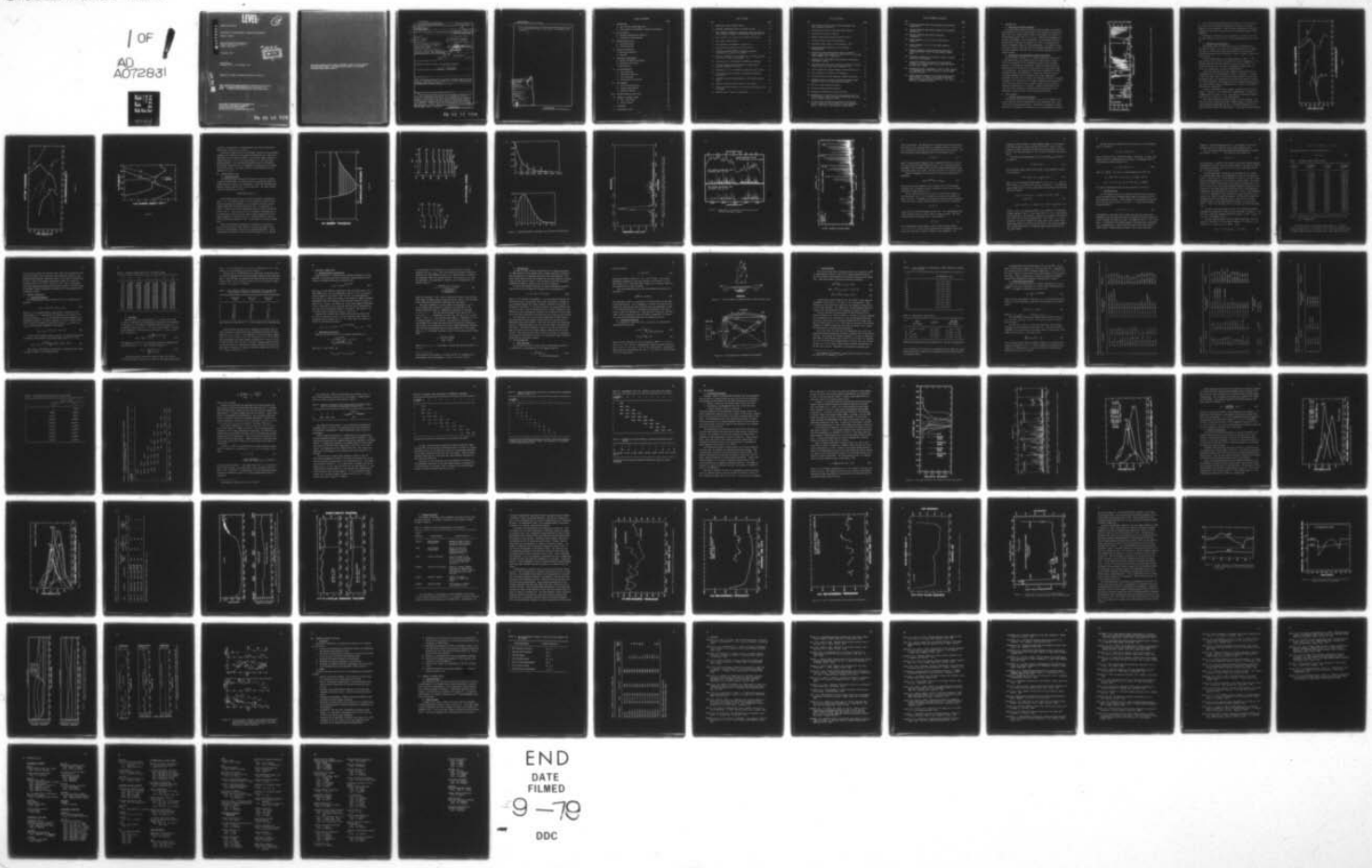

END
DATE FILMED
9-79
DDC

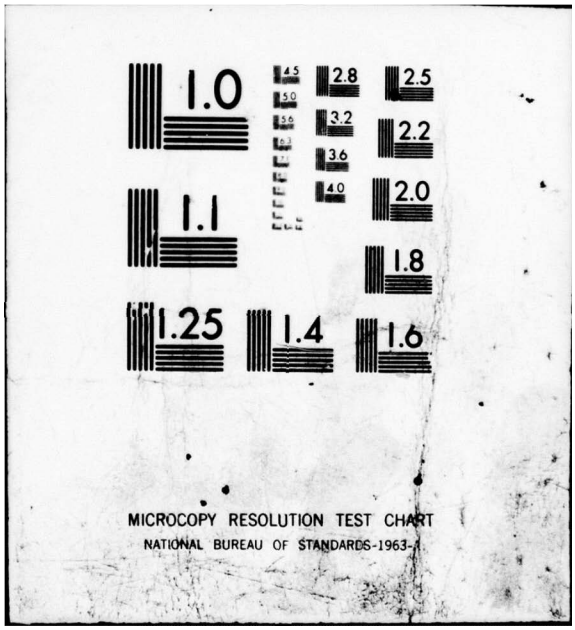
1.0
1.1
1.25
1.4
1.6
1.8
2.0
2.2
2.5
2.8
3.2
3.6
4.0
4.5
5.0
5.6
6.3
7.1
8.0
9.0
10.0
MICROCOPY RESOLUTION TEST CHART
NATIONAL BUREAU OF STANDARDS-1963-A

LEVEL II

13
B.S.

AFGL-TR-78-0251

STUDIES OF ATMOSPHERIC INFRARED EMISSIONS

Doran J. Baker

Electro-Dynamics Laboratories
Utah State University UMC 41
Logan, Utah 84322

1 January 1978

Final Report
1 January 1973 - 31 December 1977

Approved for public release; distribution unlimited.

This research was sponsored by the Defense Nuclear Agency under the subtask I25AAXY/X960, Work Unit number 02, entitled, "Advanced Test Assessment-Data Interpretation."

AIR FORCE GEOPHYSICS LABORATORY
AIR FORCE SYSTEMS COMMAND
UNITED STATES AIR FORCE
HANSCOM AFB, MASSACHUSETTS 01731

62710H

Unclassified

SECURITY CLASSIFICATION OF THIS PAGE (When Data Entered)

REPORT DOCUMENTATION PAGE

READ INSTRUCTIONS BEFORE COMPLETING FORM

1. REPORT NUMBER: AFGL-TR-78-0251
2. GOVT ACCESSION NO.
3. RECIPIENT'S CATALOG NUMBER
4. TITLE (and Subtitle): Studies of Atmospheric Infrared Emissions
5. TYPE OF REPORT & PERIOD COVERED: Scientific - Final rept. 1 Jan 73 — 31 Dec 77
6. PERFORMING ORG. REPORT NUMBER
7. AUTHOR(s): Doran J. Baker
8. CONTRACT OR GRANT NUMBER(s): F19628-73-C-0048
9. PERFORMING ORGANIZATION NAME AND ADDRESS: Electro-Dynamics Laboratories, Utah State University UMC 41, Logan, Utah 84322
10. PROGRAM ELEMENT, PROJECT, TASK AREA & WORK UNIT NUMBERS: 61102F; CDNA I25AAXY
11. CONTROLLING OFFICE NAME AND ADDRESS: Air Force Geophysics Laboratory, Hanscom Air Force Base, Massachusetts 01731, Contract Monitor: Dean Kimball/OPR
12. REPORT DATE: 1 Jan 78
13. NUMBER OF PAGES: 85
14. MONITORING AGENCY NAME & ADDRESS (if different from Controlling Office): 86 p.
15. SECURITY CLASS. (of this report): Unclassified
15a. DECLASSIFICATION/DOWNGRADING SCHEDULE

16. DISTRIBUTION STATEMENT (of this Report)

Approved for public release; distribution unlimited

24, X961

17. DISTRIBUTION STATEMENT (of the abstract entered in Block 20, if different from Report)

18. SUPPLEMENTARY NOTES

This research was sponsored by the Defense Nuclear Agency under the subtask I25AAXYX960, Work Unit number 02, entitled, "Advanced Test Assessment-Data Interpretation."

19. KEY WORDS (Continue on reverse side if necessary and identify by block number)

20. ABSTRACT (Continue on reverse side if necessary and identify by block number)

This contract between the Air Force Geophysics Laboratory and Utah State University provided for the investigation into the nature of the disturbed and undisturbed atmosphere with particular emphasis placed upon the spectral, spatial, and temporal behavior of atmospheric emission and the controlling stimuli that initiate such emission. A major thrust was concentrated on the development CONT'

DD FORM 1 JAN 73 1473 EDITION OF 1 NOV 65 IS OBSOLETE

UNCLASSIFIED

SECURITY CLASSIFICATION OF THIS PAGE (When Data Entered)

123 870

79 08 15 028

of new instrumentation and measuring techniques and their use in the measurement program, particularly in atmospheric disturbances.

TABLE OF CONTENTS

LIST OF TABLES

LIST OF FIGURES

LIST OF FIGURES (continued)

I. INTRODUCTION

A. Near Infrared (SWIR) Emissions

The vibrationally-excited OH radical, which persists at concentrations between 10^4 and 10^6 molecules/cm^3 in the region of the mesopause, gives rise to an intense (about 2 MR/μm) band sequence of airglow in the wavelength region from 2.6 to 4.4 μm. Predictable enhancements of an order of magnitude have been observed. Auroral energy deposition, gravity waves, lasering, and changes of O_3 and O concentrations are among the suggested causes of these enhancements. The computer codes need to be evolved, based upon actual OH airglow measurements, in order to predict enhanced conditions due to artificially-induced as well as natural causes.

B. Stratosphere and Mesosphere Aerospace Environment

The OH radical, although it is a minor constituent, involves both an odd oxygen and an odd hydrogen atom and thereby plays a central role in the chemistry of the troposphere and the D and E altitude regions. The production, destruction, excitation, and deactivation mechanisms in the context of the large matrix of process paths needs to be understood. The hydration of ozone and the oxidation of water, hydrogen peroxide and perhydroxyl to produce OH, important links in the oxygen-hydrogen reactive chemical cycle, occur under poorly understood circulation and vertical eddy diffusion conditions. Detailed knowledge of the constituents of the upper atmosphere and an understanding of how they interact with one another (reaction rates and their temperature dependence) are necessary. Computer-aided modeling can then provide the capability of predicting the future state of the atmospheric medium in which the Air Force systems operate.

II. THE OH RADICAL

A. Diatomic Heteronuclear Molecule

The hydroxyl free radical belongs to the class of atmospheric diatomic molecules which are nonhomonuclear and consequently have a nonzero electric dipole moment matrix. The molecule therefore is a good antenna for the emission and reception of the electromagnetic radiation.

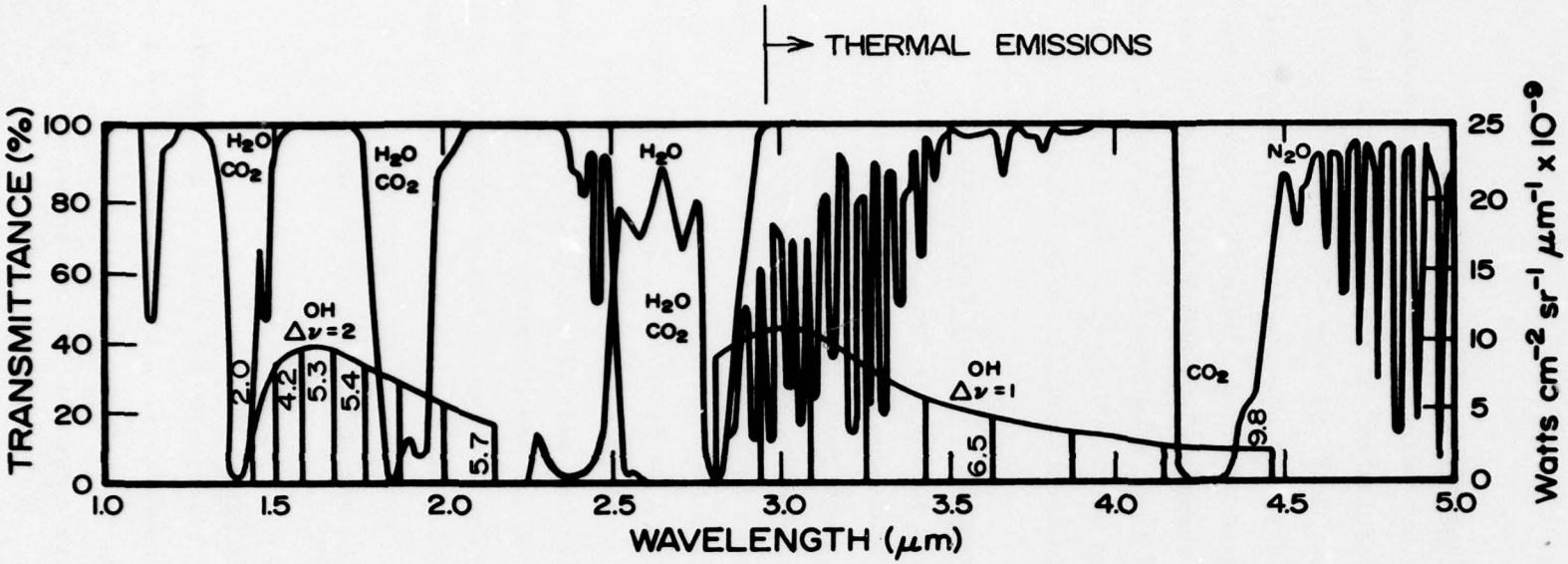

Figure 1. Near-infrared emission region where fundamental and first overtone of OH emit.

The characteristic vibration-rotation spectra of the OH molecule, which occur at near infrared wavelengths, are known as the Meinel sequences and are extensive. These emissions constitute the brightest component of the night airglow (other than nonchemiluminescent thermal emissions).

The energy of formation of the OH molecule is 0.401 eV. The dissociation energy of OH is 4.395 eV, and the ionization energy is 12.94 eV.

B. Atmospheric Concentrations

Odd hydrogen plays an important role in the recombination of odd oxygen on Earth. Also, one sink of atmospheric HO_x is the escape into space of H which has crucial implications in the evolution of planetary atmospheres and the presence of water in liquid or vapor form on the planet.

In the daytime, OH has a peak number density of about $\times 10^7$ molecules/cm^3 at an altitude of around 30 km in the troposphere. It is produced primarily from the oxidation of H_2O and H_2 by $O(^1D)$. The concentration drops off two orders of magnitude at about 70 km. At 85 km, the concentration is about 10^5 molecules/cm^3.

During the night-time the number density of OH molecules in the troposphere drops off approximately an order of magnitude. At 85 km, on the other hand, which is about the altitude region of the infrared OH airglow layer, the concentration rises just after sunset to nearly 2×10^5 molecules/cm^3. There appears to be a secondary maximum at about the 85-km altitude, above a minimum which is at about 50 km (compared with 70 km in the daytime).

By way of comparison the H_2O and HO_2 concentrations at 85 km are about 4×10^6 and 4×10^4 molecules/cm^3, respectively. The H_2O_2 has a number density of only 4×10^3. The atomic H concentration peaks at about 90 km at a value of 6×10^8 molecules/cm^3.

The ozone concentration profile appears to have two maxima. The major one occurs at about 30 km with a number density in excess of 10^{12} which persists through night and day. A secondary maximum occurs at about 85 km with nearly 10^7 molecules/cm^3. The salient diurnal variation

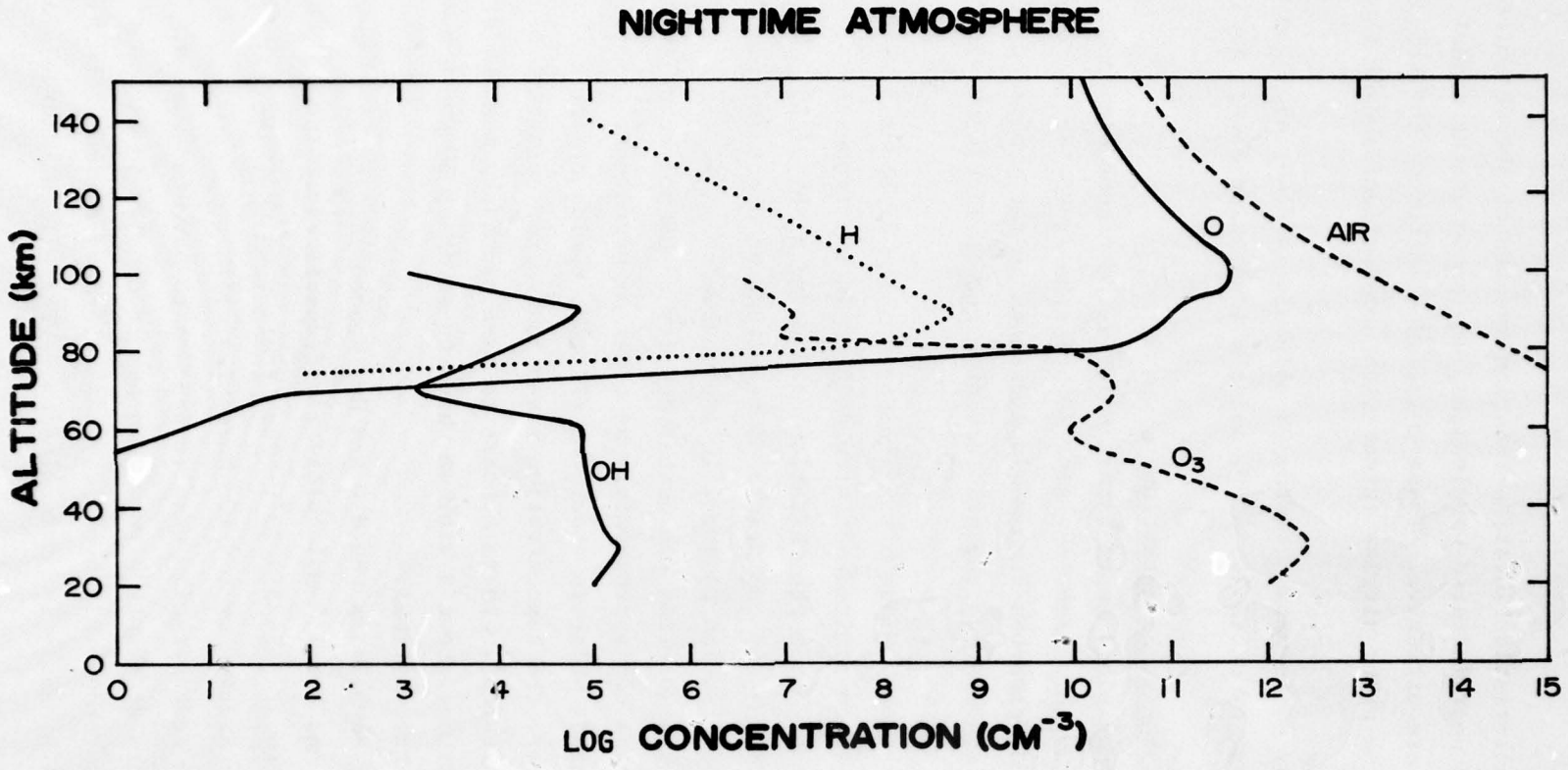
NIGHTTIME ATMOSPHERE
ALTITUDE (km)
140
120
100
80
60
40
20
0
0
1
2
3
4
5
6
7
8
9
10
11
12
13
14
15
LOG CONCENTRATION (CM^{-3})
H
O
AIR
OH
O_3

Figure 2.

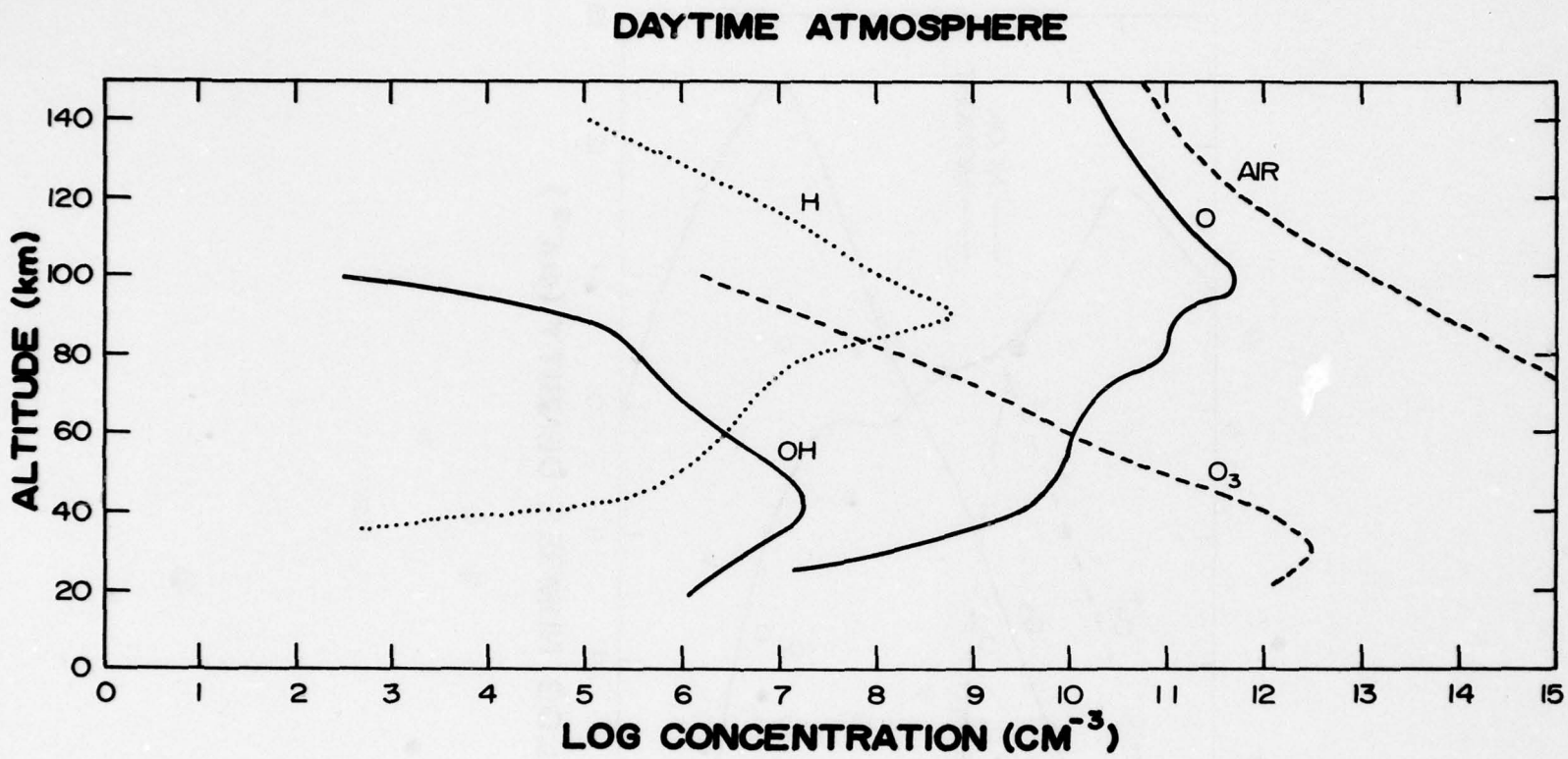
DAYTIME ATMOSPHERE
ALTITUDE (km)
140
120
100
80
60
40
20
0
0 1 2 3 4 5 6 7 8 9 10 11 12 13 14 15
LOG CONCENTRATION (CM^{-3})
H
OH
O
AIR
O_3

Figure 3.

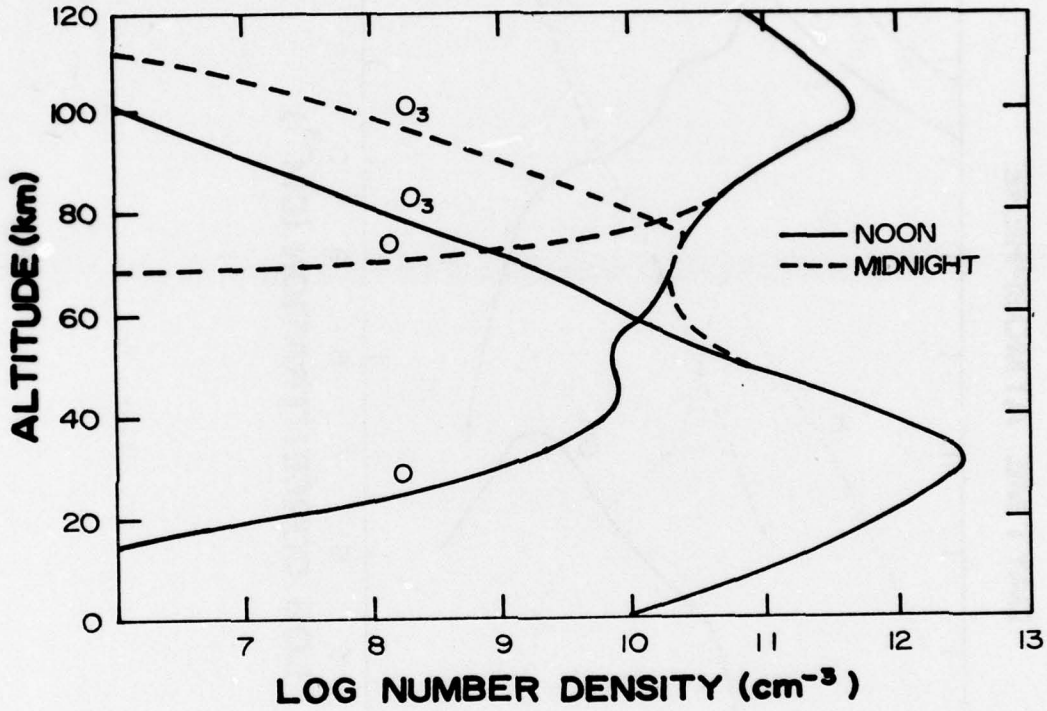
120
100
80
60
40
20
0
ALTITUDE (km)
7
8
9
10
11
12
13
LOG NUMBER DENSITY (cm⁻³)
O₃
O₃
O
O
NOON
MIDNIGHT

Figure 4.

of the O_3 concentration is a sharp decrease just after sunrise which takes three or four hours to recover.

The atomic oxygen, which is the "kingpin" species in the mechanisms leading to the formation and quenching of excited OH, has a peak concentration in the vicinity of 100 km. At 85 km the number density of O ranges from about 3×10^{11} just after sunset to 3×10^{7} just before morning twilight. The electronically-excited state $O(^1D)$ formed by the sunlight photolysis of O_2 is important in forming OH by the oxidation of H_2O or H_2O_2. The ozone at 85 km is formed primarily by the oxidation of O_2 by O.

III. EXCITED STATES OF OH

A. Rotating Vibrator

The hydroxyl Meinel sequences of radiation in the near infrared airglow are attributable to vibration-rotation transitions within the ground electronic state of the OH molecule. Electronic absorption and emission spectra from OH occur in the ultraviolet. The lowest energy electron configuration for OH is

$$K(2s\sigma)^2(2p\sigma)^2(2p\pi)^3\ {}^2\Pi_i \quad .$$

This ground electronic state for the OH molecule is designated Π since $\Lambda = 1$. The quantum number Λ is that associated with the vector $\vec{\Lambda}$ which represents the component of the resultant electronic orbital angular momentum $\vec{L}$ along the internuclear axis. Its magnitude is $\Lambda(h/2\pi)$. This state is doubly degenerate because of the two possibilities $+\Lambda$ and $-\Lambda$. This gives rise to the so-called Λ splitting due to the interaction of the electronic orbital angular momentum $\vec{L}$ with the angular momentum of nuclear rotation $\vec{N}$. At high speeds of rotation, this Λ splitting can approach 1 cm^{-1} in difference of rotational energy level.

Since the OH molecule possesses an odd number of electrons, it has an even multiplicity 2S+1, where S is the quantum number corresponding to the resultant electronic spin angular momentum $\vec{S}$. As the total number of electrons is odd, S is half integral ($S = \frac{1}{2}$), and the

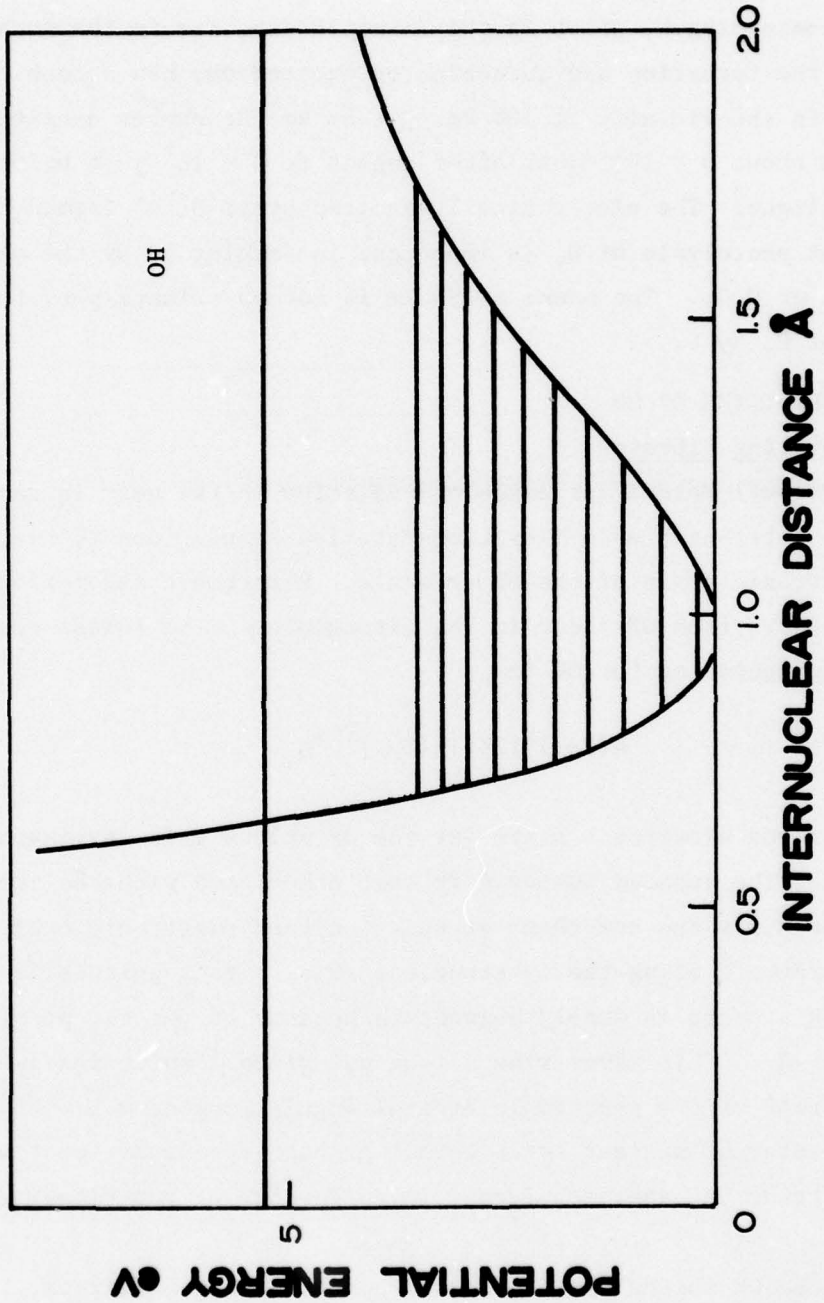
OH
POTENTIAL ENERGY eV
5
0
0.5
1.0
1.5
2.0
INTERNUCLEAR DISTANCE Å

Figure 5.

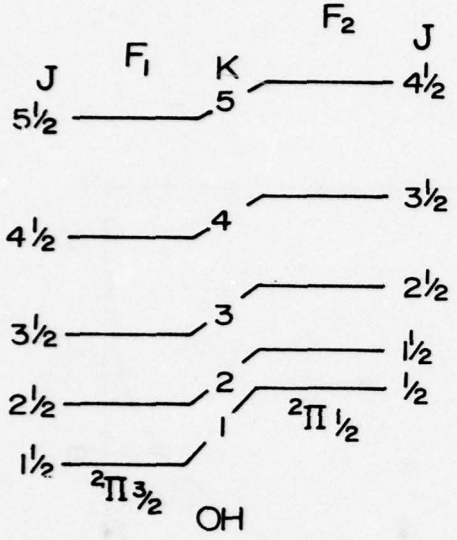

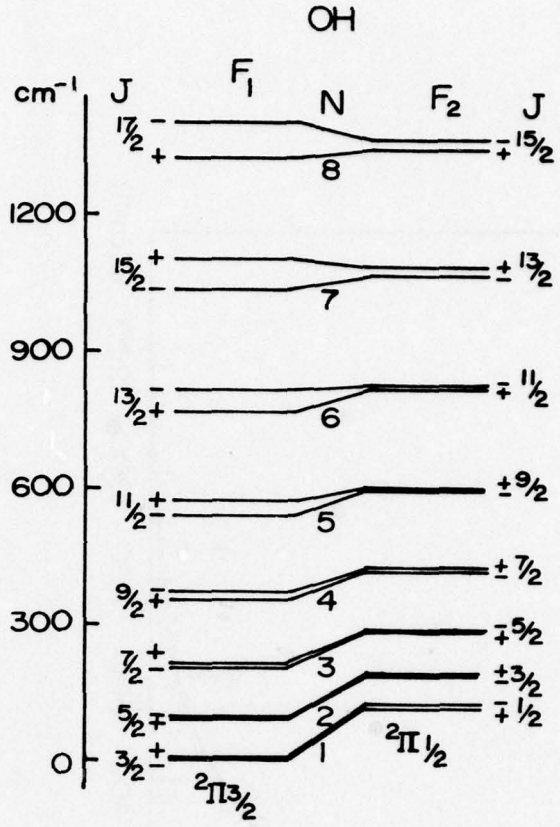

OH ROTATIONAL STATES

Figure 6.

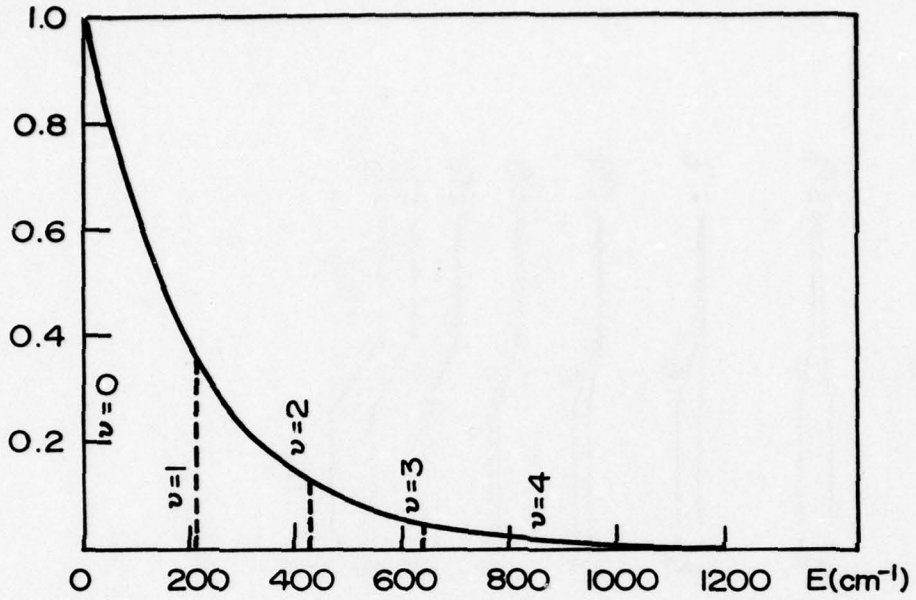

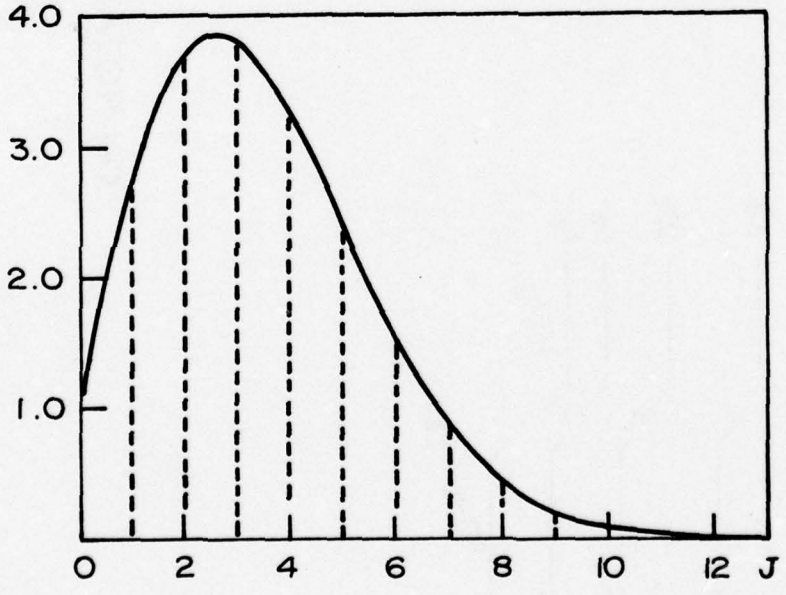

Figure 7. Maxwell-Boltzmann vibrational and rotational distributions.

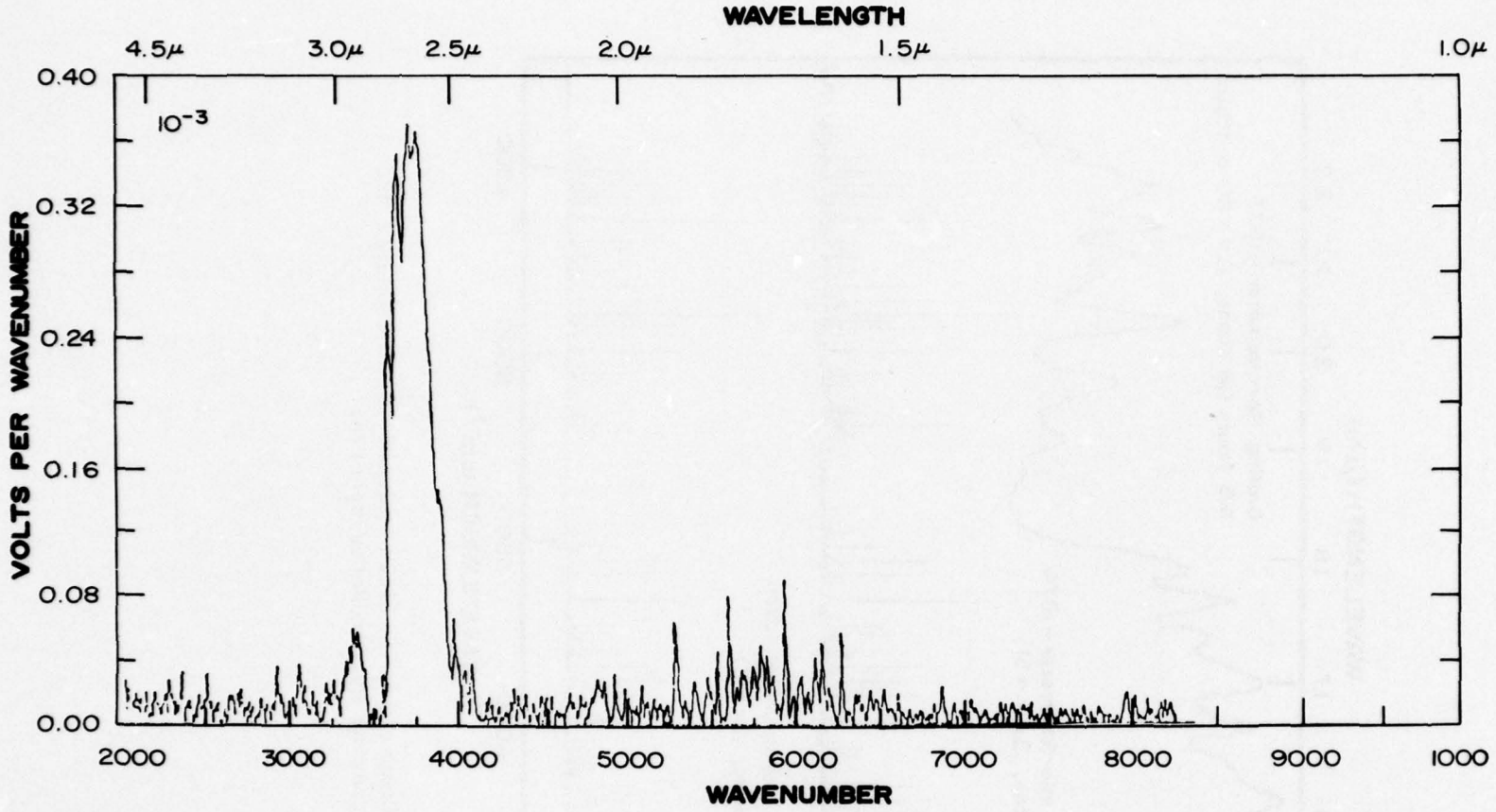

Figure 8. Spectrum of zenith near-infrared emission spectrum taken at Poker Flat, Alaska, on 5 April 1973 (8 ten-second scans coadded, 9 cm^{-1} resolution).

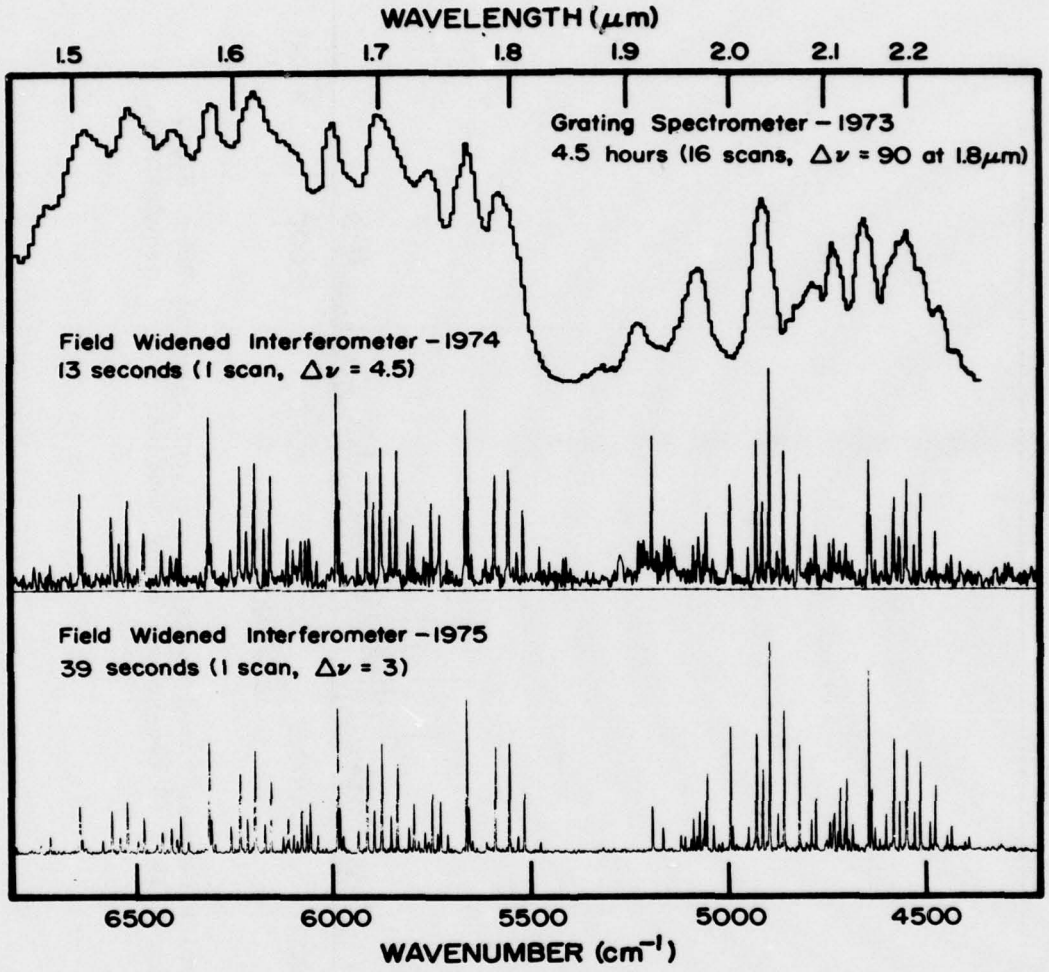

Figure 9. Comparison of field-widened interferometer and grating spectrometer spectra.

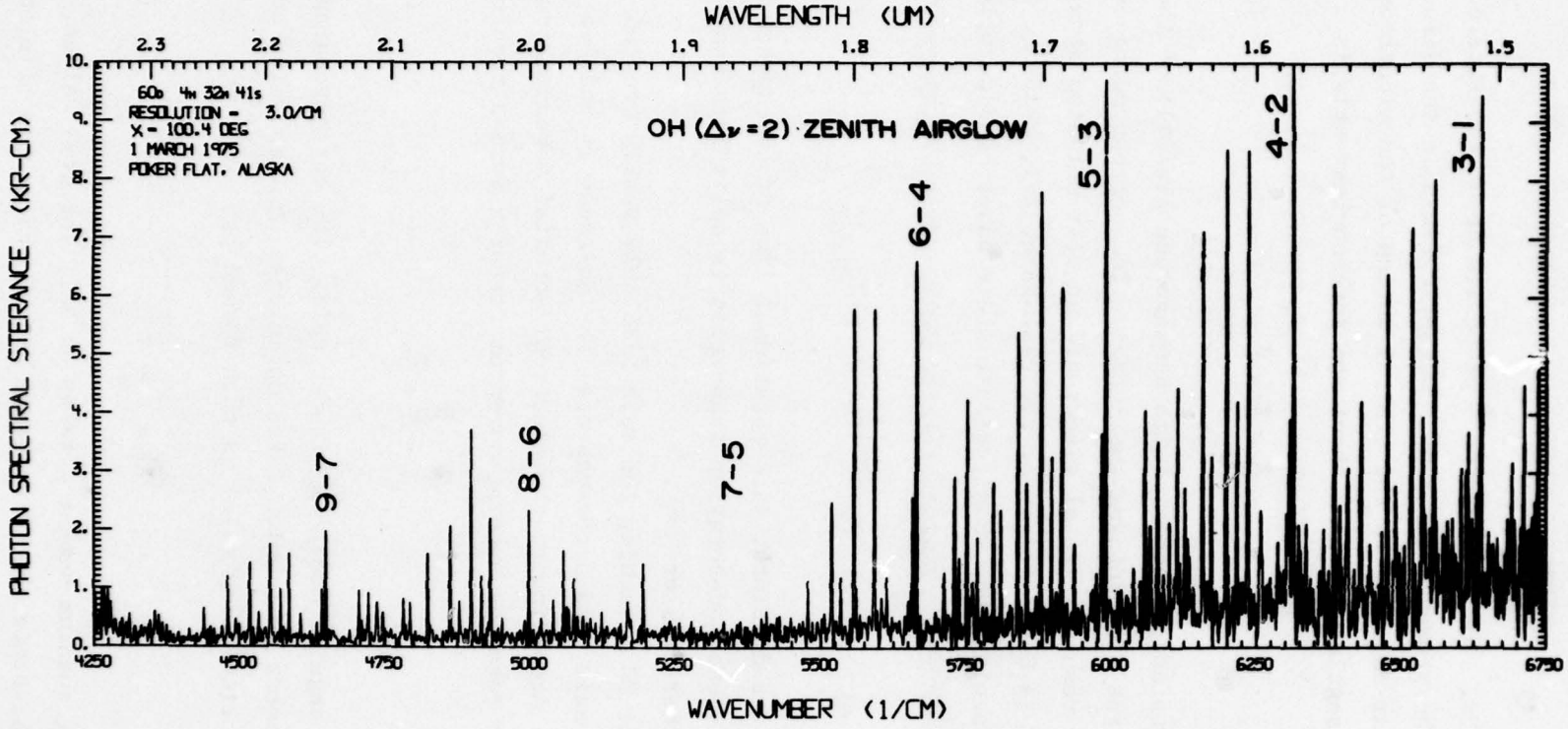

Figure 10. Instrument-corrected zenith radiance of OH(Δv=2) measured from the ground at Poker Flat, Alaska, March 1, 1975.

states are doublets. The spin vector $\vec{S}$ precesses about the internuclear axis because of the presence ($\Lambda \neq 0$) of a magnetic field in the direction of the internuclear axis due to the orbital motion of the electrons. The total electronic angular momentum about the internuclear axis is

$$\vec{\Omega} = \vec{\Lambda} + \vec{\Sigma} \qquad (1)$$

where $\vec{\Sigma}$ is the constant component [with a magnitude $\Sigma(h/2\pi)$] of the vector spin $\vec{S}$ along the line joining the nuclei. The corresponding quantum number of the resultant total electronic angular momentum about the internuclear axis is $\Omega = |\Lambda+\Sigma|$. For the case here, $\Lambda=1$, $\Sigma=\pm S=\pm 1/2$, $\Omega=3/2, 1/2$.

From the foregoing, the OH electronic state under consideration is designated

$$[\text{el.st.}]^{2S+1}[\Lambda]_{\Omega} \rightarrow X^2\Pi_{3/2,1/2} \quad . \qquad (2)$$

Since the states are doublets, each rotational line of the spectrum resulting from a vibration-rotation transition is split into two lines according to whether $\Omega=3/2$ or $\Omega=1/2$.

For the light OH molecule, the spin $\vec{S}$ is only weakly coupled to the internuclear axis. As a consequence, the molecule is modeled as Hund's case (b). Accordingly, the electronic orbital momentum component $\vec{\Lambda}$ and the nuclear rotation angular momentum vector $\vec{N}$ form a resultant

$$\vec{K} = \vec{\Lambda} + \vec{N} \qquad (3)$$

called the total angular momentum without spin. The corresponding rotational quantum number is K which takes on integral values. The total angular momentum (including spin) is then formed by

$$\vec{J} = \vec{K} + \vec{S} \quad . \qquad (4)$$

The corresponding quantum number J takes on half integral values, $J = K + S = K \pm 1/2$, since the OH molecule has an odd number of electrons. Thus, each level with a given K consists of two components. The

molecular rotation produces a slight magnetic moment in the direction of $\vec{K}$, which produces a small coupling of $\vec{S}$ with $\vec{K}$. This, in turn, produces a slight splitting of levels which have different J but the same K. This spin splitting ($\Omega = 3/2, 1/2$) effect increases with increasing K.

The energy levels expressed in cm^{-1} of the $X^2\Pi_{3/2,1/2}$ state of OH are given by

$$T = G(v) + F(J) \quad . \tag{5}$$

The vibrational energy values (term values) of the anharmonic oscillator are given by

$$G(v) = \omega_e(v + 1/2) - \omega_e x_e(v + 1/2)^2 + \ldots \tag{6}$$

where v is the vibrational quantum number v = 0, 1, 2,... . For the $O^{16}H^1$ isotope, $\omega_e = 3735.21\ cm^{-1}$ and $\omega_e x_e = 82.81\ cm^{-1}$. The rotational energy (term) values for the nonrigid rotator are given by the Hill and Van Vleck formulas

$$F_1(J) = B_v \{(K + 1)^2 - 1 - 1/2[4(K + 1)^2 + Y(Y - 4)]^{1/2}\} - D_v(K + 1/2)^4 \tag{7}$$

$$F_2(J) = B_v \{K^2 - 1 + 1/2[4K^2 + Y(Y - 4)]^{1/2}\} - D_v(K + 1/2)^4 \tag{8}$$

where $Y = A/B_v$. The coupling constant A is a measure of the coupling strength between $\vec{S}$ and $\vec{\Lambda}$. In the case of OH, Y = -7.41. Such doublets with a negative Y, and therefore a negative A, are said to be inverted. $F_1(J)$ and $F_2(J)$ are the term series for $J = K + 1/2$ and $J = K - 1/2$, respectively. For the OH inverted $^2\Pi$ states, the F_1 and F_2 terms correspond respectively, to the $^2\Pi_{3/2}$ and $^2\Pi_{1/2}$ states. For a given K number, the $^2\Pi_{1/2}$ spin levels form at a slightly higher energy level than the $^2\Pi_{3/2}$ spin levels.

The mean rotational constant B_v for the rotator in the vibrational state v is given by

$$B_v = B_e - \alpha_e(v + \tfrac{1}{2}) + \ldots \qquad (9)$$

where the value of B_e is calculated from $B_e = h/8\pi^2 c\mu r_e^2$. The mean rotational constant D_v representing the influence of centrifugal force is approximated for small values of v by

$$D_v = D_e + \beta_e(v + \tfrac{1}{2}) + \ldots \qquad (10)$$

where $D_e = 4B_e^3/\omega_e^2$. The values of these parameters for $O^{16}H^1$ are

$$B_e = 18.871 \text{ cm}^{-1}, \ \alpha_e = 0.714, \ r_e = 0.9706 \times 10^{-8}\text{cm},$$

$$D_e = 4.5 \times 10^{-4}, \ \beta_e = -0.65 \times 10^{-4} \text{ and } \mu = 0.948376.$$

The lowest vibrational interval for OH is 3570 cm^{-1} (0.443 eV).

B. Infrared Spectra

For the hydroxyl molecule the infrared vibration-rotation spectra can be described from the quantum values under the constraints of the following selection rules. In the airglow, the vibrational quantum number v can take on the values v = 0,1,2,3,...., 9 with allowed changes during emission of

$$\Delta v = 1, 2, 3, \ldots, 9 \qquad (11)$$

The ensemble of rotational lines, which occur near one another wavelengthwise, that are associated with the transition from one vibrational state to another are known as a band. An example is the (v', v") = (5,3) band. In transitions the quantum numbers of the upper level energywise will be designated by a single prime and those of the lower level by double primes. Bands grouped according to the Δv are called band

sequences. The band sequence with $\Delta v = 1$ is referred to as the fundamental, and $\Delta v = 2$ called the first overtone sequence, etc.

The total-angular-momentum-without-spin quantum number K can have the values K = 1,2,3,... . The selection rule, however, is

$$\Delta K = 0, \pm 1 \quad . \tag{12}$$

The collection of rotational lines within a particular band but grouped according to the value of ΔK are called branches. The branch for $\Delta K = 0$ is called the Q branch, that for $\Delta K = +1$ is the R branch and that for $\Delta K = -1$ is the P branch.

The spin splitting, arising from the multiplicity of Ω, namely, $\Omega = 3/2$ and $1/2$ gives rise to two subbranches for each of the branches Q, R and P. The set for $\Omega = 3/2$ are referred to as the Q_1, R_1 and P_1 lines. The set corresponding to $\Omega = 1/2$ are the Q_2, R_2 and P_2 lines. The further splitting of each of these lines, the so-called Λ splitting due to the use of $+\Lambda$ and $-\Lambda$ for the electronic angular momentum orientation in one direction or the other along the internuclear axis in the eigenvalue formulation, are designated by the subscripts c and d. Each designation c or d is a combination of the orientations as the eigenvalues do not separate out clearly as might be supposed. Following this scheme for designating each of the rotational lines, those of the (5,3) band listed in order of increasing wavenumber (energy) are as follows in Table 1. The K" for the lower state of each line is given in parentheses.

For large rotational quantum numbers, the Λ splitting increases approximately quadratically with K for the multiplet $^2\Pi_i$ states, i = c,d. For the P_1 lines the wavenumber difference $\Delta\sigma_{cd}(K) = F_{1\,c}(K) - F_{1\,d}(K)$, is less than a wavenumber for $K < 6$.

The total angular momentum quantum number (with spin) J has two values for each value of K according to whether $\Omega = 3/2$ (the P_1, Q_1, R_1 lines) or $\Omega = 1/2$ (the P_2, Q_2, R_2 lines). Thus,

$$J = K + 1/2 = 1\tfrac{1}{2},\ 2\tfrac{1}{2},\ 3\tfrac{1}{2},\ \ldots\ (\Omega = 3/2) \tag{13}$$

$$J = K - \tfrac{1}{2} = \tfrac{1}{2},\ 1\tfrac{1}{2},\ 2\tfrac{1}{2},\ \ldots.\ (\Omega = \tfrac{1}{2})$$

The selection rules on J are the same as for K,

$$\Delta J = 0, \pm 1 \qquad (14)$$

Table 1. Rotational lines of OH(5,3) band.

Rotational Line	Wavenumber $\sigma(cm^{-1})$	Rotational Line	Wavenumber $\sigma(cm^{-1})$
$P_{1d}(6)$	5,751.34	$P_{2d}(2)$	5,937.95
$P_{1c}(6)$	5,752.83	$P_{2c}(2)$	5,940.15
$P_{1d}(5)$	5,797.07	$Q_{1c}(2)$	5,984.52
$P_{1c}(5)$	5,797.17	$Q_{1d}(2)$	5,985.89
$P_{2d}(5)$	5,810.11	$Q_{1c}(1)$	5,990.12
$P_{2c}(5)$	5,810.34	$Q_{1d}(1)$	3,990.76
$P_{1d}(4)$	5,839.74	$Q_{2d}(1)$	5,992.25
$P_{1c}(4)$	5,839.84	$Q_{2c}(1)$	5,992.75
$P_{2d}(4)$	5,855.17	$R_{1d}(1)$	6,059.43
$P_{2c}(4)$	5,855.22	$R_{1c}(1)$	6,059.61
$P_{1d}(3)$	5,879.26	$R_{2d}(2)$	6,068.04
$P_{1c}(3)$	5,879.33	$R_{2c}(2)$	6,070.22
$P_{2d}(3)$	5,897.84	$R_{1d}(2)$	6,081.88
$P_{2c}(3)$	5,898.83	$R_{1c}(2)$	6,082.52
$P_{1d}(2)$	5,915.67	$R_{1c}(3)$	6,101.19
$P_{1c}(2)$	5,916.58	$R_{1d}(3)$	6,101.60

Notes: ( )→K"; P→ΔK = -1; Q→ΔK = 0; R→ΔK = +1; 1→Ω= $\frac{3}{2}$; 2→Ω = $\frac{1}{2}$; c,d→ ± Λ combination.

Since the values of the quantum number K begin at 1, and the P lines correspond to ΔK = 1, the first P line that can be observed in OH is P(K=2) where K refers to the lower state. Thus, there are no $P_1(1)$

or $P_2(1)$ lines, giving the "missing tooth" effect in the spectrum of OH. The Q and R lines, on the other hand, begin with Q(1) and R(1). The spacing between adjacent rotational levels (of the same Ω) is about $2B_e$. For the P_1 lines of the OH(5,3) band whose Q center is at 5991 cm^{-1} (1.669 μm) this is $\Delta\sigma = F_1(3) - F_1(2) = 37\ cm^{-1}$. Due to centrifugal force this spacing increases with increasing K values. For the R_1 lines of the OH(5,3) band the separation is about 22 cm^{-1} and decreases with increasing K values.

IV. EMMISION INTENSITIES

A. Spontaneous Emission

The volume emission rate in photons $s^{-1}cm^{-3}$ of a central line is given by

$$I_{v'J',\ v''I''} \approx N_{v'J'}\ A_{v'J',\ v''J''} \quad , \tag{15}$$

where $N_{v'J'}$ is the number density (population) of molecules in the initial state v', J' carrying out the transition to the state v", J". The coefficient $A_{v'J',\ v''J''}$ is the Einstein transition probability of spontaneous emission. In order to express I in terms of power (intensity) it would be necessary to multiply by $hc\sigma_{v'J',\ v''J''}$ where $\sigma_{v'J',\ v''J''}$ is the wavenumber (frequency) of the photon

$$\sigma_{v'J',\ v''J''} = F(v',\ J') - F(v'',\ J'') \tag{16}$$

For the case of electric dipole radiation the Einstein coefficient is related to the element of the dipole moment matrix $R^{v'J',v''J''}$ by

$$A_{v'J',\ v''J''} = \frac{64\ \pi^4(\sigma_{v'J',\ v''J''})^3}{3h}\ \left|R^{v'J',\ v''J''}\right|^2 \tag{17}$$

The values of the Einstein coefficients as computed by Mies [1974] are given in Table 2 for the OH(5,3) band.

Table 2. Einstein coefficients (sec^{-1}) for OH(5,3) band.

J'	P_1	Q_1	R_1	P_2	Q_2	R_2
0.5	0.000	0.000	0.000	72.290	35.341	0.000
1.5	45.622	61.574	0.000	67.099	7.749	32.736
2.5	55.591	25.180	26.464	65.770	3.748	37.896
3.5	59.653	13.263	34.190	65.638	2.360	39.065
4.5	61.967	7.995	36.808	65.970	1.685	38.856
5.5	63.575	5.255	37.398	66.487	1.289	37.990
6.5	64.824	3.673	36.996	67.063	1.029	36.751
7.5	65.850	2.687	36.042	67.634	0.844	35.275
8.5	66.715	2.038	34.751	68.166	0.707	33.642
9.5	67.436	1.590	33.229	68.634	0.600	31.891
10.5	68.057	1.270	31.577	69.039	0.516	30.075
11.5	68.567	1.034	29.823	69.362	0.448	28.206
12.5	68.967	0.855	27.999	69.595	0.393	26.302
13.5	68.259	0.717	26.128	69.733	0.346	24.377
14.5	69.444	0.609	24.230	69.772	0.307	22.445
15.5	69.521	0.521	22.319	69.709	0.273	20.518

B. Lifetimes

The mean life of an excited state v', J' is that time τ that it takes, in the absence of quenching and production of new molecules in the state, for the number of molecules left in the state v', J' to decrease e-fold, that is, to $1/e$ of the initial number. The exponential decrease of the molecules in the state v', J' due to radiative relaxation is

$$N_{v'J'} = N^{\circ}_{v'J'}\, e^{-\left(\sum_{v''J''} A_{v'J',v''J''}\right)t} \qquad (18)$$

The summation is over all of the possible transitions downward from the initial state v', J'. Thus, the mean lifetime is

$$\tau_{v'J'} = \frac{1}{\sum_{v''J''} A_{v'J',v''J''}} \quad . \qquad (19)$$

Using the Einstein coefficient values of Mies (see Table 8), the mean lifetime of a particular v'-state of $OH^{\ddagger}$ ranges from 3.3 msec

for v' = 9, to 8.1 msec at v' = 5, up to τ = 50 msec for v' = 1. The results of the calculations are given in Table 3.

The mean age of an $OH^{\ddagger}$ molecule in a particular vibrational level can also be approximated ignoring quenching, assuming a given injection level. These $OH^{\ddagger}$ ages are computed (see Table 10) and the results tabulated in Table 3 for the cases of injection of the vibrational energy at the v' = 9 or the v' = 6 levels.

Table 3. Mean radiative lifetime of vibrational state and mean age since original formation of $O^{\ddagger}$ molecule relaxing from v'.

v'	Lifetime τ (msec)	Age, v'→9 (msec)	Age, v'→6 (msec)
9	3.3	3.3	--
8	3.9	7.2	--
7	4.7	8.2	--
6	6.0	10.4	6.0
5	8.1	14	14
4	11.1	17	17
3	16.2	24	23
2	25.4	35	33
1	49.6	63	60

Age is given for injection at v' = 9 and 6 levels for no quenching case.

These lifetimes and ages can be compared with the mean times between collisions of OH molecules with the ambient molecules and atoms, primarily N_2, O_2, A and O. The atmospheric collision frequency ranges from 1.4×10^5 at 75 km, to 2.2×10^4 at 85 km, to 1.2×10^3 at 100 km. The corresponding mean times between collisions are 7.1 μsec at 75 km, 45 μsec at 85 km, and 0.83 msec at 100 km. Using the ages from Table 3, the mean number of collisions with ambient molecules at 85 km before mean time of occurrence of radiative relaxation ranges from 70 for the v' = 9 level to 1400 for v' = 1.

V. ROTATIONAL TEMPERATURES

A. Maxwell-Boltzmann Distribution

Under conditions of rotational state thermal equilibrium, the distribution of the molecules over the different quantum numbers is described by the Maxwell-Boltzmann distribution law,

$$N_{v'J'} = C_{v'} w_{J'} e^{-E_{v'J'}/kT} \tag{20}$$

where $N_{v'J'}$ is the number of molecules in the rotational state J' of a vibrational level v' at the temperature T and $w_{J'} = 2J' + 1$ is the statistical weight of the state J' with its (2J' + 1)-fold degeneracy. The constant $C_{v'}$, whose actual value is not needed to compute rotational temperatures from the intensity of the rotational lines of a band, is given by $C_{v'} = N_{v'}/Q_r = N_{v'}kT/hcB$; $N_{v'}$ is the total number of molecules in the v level and Q_r is the partition function (sum of Boltzmann factors over all the rotational states of the level). The energy of the rotational state is designated by $E_{v'J'} = F_{v'}(J')hc$.

Equation (20) inserted into Equation (15) gives the volume emission rate (in photons $sec^{-1}cm^{-3}$) of each rotational line arising in transitions from an upper state v'J' to a lower state v"J" under conditions of rotational equilibrium.

$$I_{v'J',\ v"J"} = C_{v'}(2J' + 1)e^{-F_{v'}(J')hc/kT} A_{v'J',\ v"J"} \tag{21}$$

B. Temperature Calculation

Equation (21) when solved for the absolute temperature T is

$$T = \frac{F_{v'}(J')hc/k}{\ln\left[\dfrac{R_{v'J',v"J"}}{C_{v'}(2J'+1)A_{v'J',v"J"}}\right]} \ (°K) \tag{22}$$

where $hc/k = 1.439\ °K/cm^{-1}$ and

$$R_{v'J',v"J"} = I_{v'J',\ v"J"}/4\pi \tag{23}$$

is the radiance (in rayleighs*) of the rotational line of volume emission rate $I_{v'J',\ v''J''}$. With this equation the apparent rotational temperature of any observed OH band can be computed using a minimum of two rotational lines (of the same branch). The constant $C_{v'}$ can thus be eliminated. The temperature, therefore, can be computed from the absolute value of

$$T = \frac{(hc/k)[F_{v'}(J_1') - F_{v'}(J_2')]}{\ln\left|\frac{R_1(2J_2'+1)A_2}{R_2(2J_1'+1)A_1}\right|} \tag{24}$$

where the subscripts 1 and 2 refer to the two rotational lines selected (with upper rotational states J_1' and J_2') and $R_{1,2}$ and $A_{1,2}$ are the appropriate radiances and Einstein coefficients for the lines.

The usual procedure is to plot values of $\ln[R_K(2J_K'+1)^{-1}\ A_K^{-1}]$ as an ordinate value versus hc $F_{v'}(J_K')/k$ as the abscissa for the various rotational lines of a branch whose radiances are observed, K = 1, 2, 3, ... For the relatively bright $P_1(K)$ lines of OH, K = 2, 3, 4, 5, ... Furthermore, for this $^2\Pi_{3/2}$ case $J_K' = K'+\frac{1}{2}$, so that $2J_K' + 1 = 2(K' + 1)$. Thus, for the $P_1(K)$ lines, $x = \ln[R_K(K'+1)^{-1}\ A_K^{-1}]$ is plotted versus $y = hc\ F_{v'}(K')/k$. The negative of the slope of the straight line through the points gives the rotational temperature T. Due to noise, or any departure from an exact Maxwell-Boltzmann distribution, the best approximation may be a least squares fit of a straight line $y = y_o - Tx$ through the points, where b is the slope given by [*Ware*, 1976]

$$T = \frac{\Sigma x_i\ \Sigma y_i - n\Sigma x_i y_i}{n\Sigma x_i^2 - (\Sigma x_i)^2} \tag{25}$$

where n = 1, 2, 3, ... is the number of points and each sum is from n = 1 to n = i.

---

*The conversion from radiance L in watts $cm^{-2}sr^{-1}$ to rayleighs for a monochromatic line of wavenumber σ in cm^{-1} is $R = 2\pi L \times 10^{17}/\sigma$.

C. Equilibration

In order for the rotational distribution to be Maxwell-Boltzmann, the $OH^{\ddagger}$ molecules on the average have to undergo sufficient collisions with the ambient N_2 to approach rotational state equilibration. One would expect that not less than perhaps ten collisions would be required. Using the ages given in Table 3, the altitude at which $OH^{\ddagger}$ rotational equilibration might be expected to occur can be estimated.

The mean time between collisions of neutral atmospheric molecules versus altitude in the region of interest may be approximated by

$$\tau = 4.4 \times 10^{-12}\ e^{0.19h}\ \text{(sec)} \qquad (25b)$$

where h is the altitude in kilometers. For the promptly-radiating 9th vibrational state, the altitude level which corresponds to averages of ten collisions during the 3.3-msec radiative lifetime of the level is estimated to be 120 km. At the other extreme, the average $OH^{\ddagger}$ molecule in the v'=1 state, with the 63-msec age since original formation of the $OH^{\ddagger}$ molecule which subsequently cascaded, can be expected to have experienced some 1400 collisions if the molecules were located as low as 80 km.

It would appear that the rotational temperature of $OH^{\ddagger}$ radiation emanating from altitude regions around 85 km would effectively be in Maxwell-Boltzmann distributions. Seen from the ground, the temperature would be an integrated effect over the altitude range of the optically-thin layer. This layer thickness is about 10 km, with the peak dropping from about 87 km for the night airglow to about 83 km for the day airglow. This altitude shift must be taken into account in assessing the rotational temperature as a measure of the ambient upper atmospheric temperature of the neutral species.

VI. OH PHOTOCHEMISTRY

A. Ozone Hydration

By the *Bates* and *Nicolet* [1950] theory vibrationally excited OH is produced by the exothermicity of the chemical reaction

$$H + O_3 \xrightarrow{k_1} OH^{\ddagger} + O_2 \qquad (26)$$

(+3.3 eV=78 kcal/mole)

The rate constant

$$k = aT^b e^{c/T} \tag{27}$$

is given by *Nicolet* [1972] as $a = 1.5 \times 10^{-12}$ cm^3/sec. The kinetic temperature dependence of the rate constant is estimated at $b = 0.5$. Some [*Blank et al.*, 1974] have given a value of c as high as 500°K; for our purposes we will take it as zero.

Thus, the production rate by the ozone hydration process can be described by

$$d[OH^{\ddagger}]/dt = k[H][O_3] \tag{28}$$

The night-time H and O_3 concentrations at 85 km are both on the order of 10^8 molecules/cm^3. For a temperature of 220°K, the production rate computed by ignoring all other production and loss mechanisms is about 2×10^5 molecules sec^{-1}cm^{-3}. Observations [*Krassovsky*, 1963] give a yield of nearly 10^6 $OH^{\ddagger}$/sec-cm^3. Under day-time conditions, with the O_3 number density decreased by some two orders of magnitude, the production rate of vibrationally-excited OH is likewise much lower.

B. Perhydroxyl Reduction

The oxidation or hydration of HO_2 can lead to the formation of vibrationally-excited OH,

$$O + HO_2 \xrightarrow{k_2} OH^{\ddagger} + O_2 \quad (+2.3 \text{ eV}=54 \text{ kcal/mole}) \tag{29}$$

$$H + HO_2 \xrightarrow{k_3} OH^{\ddagger} + OH \tag{30}$$

where the rate constants are given by [*Kaufman*, 1969] $k_2 = 1 \times 10^{-11}$ and $k_3 = 3 \times 10^{-12}$ cm^3/sec. Representative night-time number densities are 2×10^{11}, 2×10^8, and 2×10^5 for [O], [H] and [HO_2], respectively, $OH^{\ddagger}$ production rates therefore are about 4×10^5 and 1.2×10^2 molecules sec^{-1}cm^{-3}, respectively.

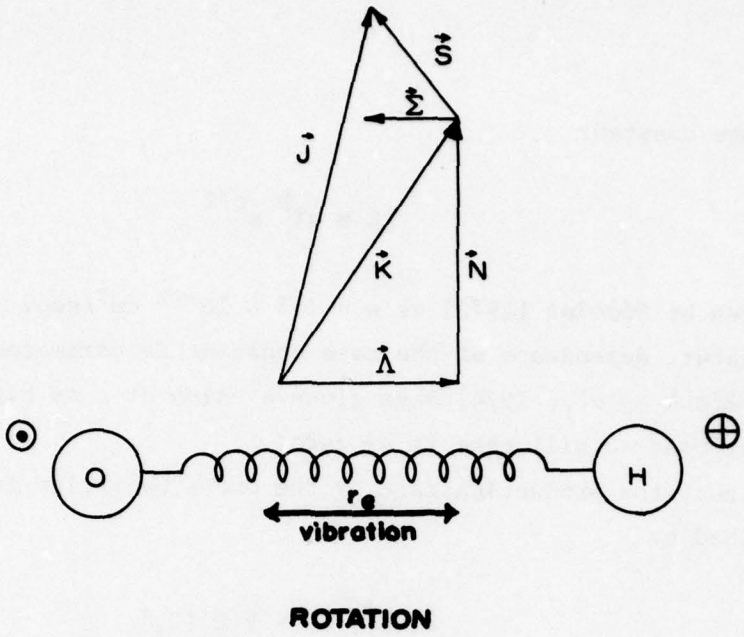

Figure 11. Vector diagram for angular momenta of OH vibrating rotor.

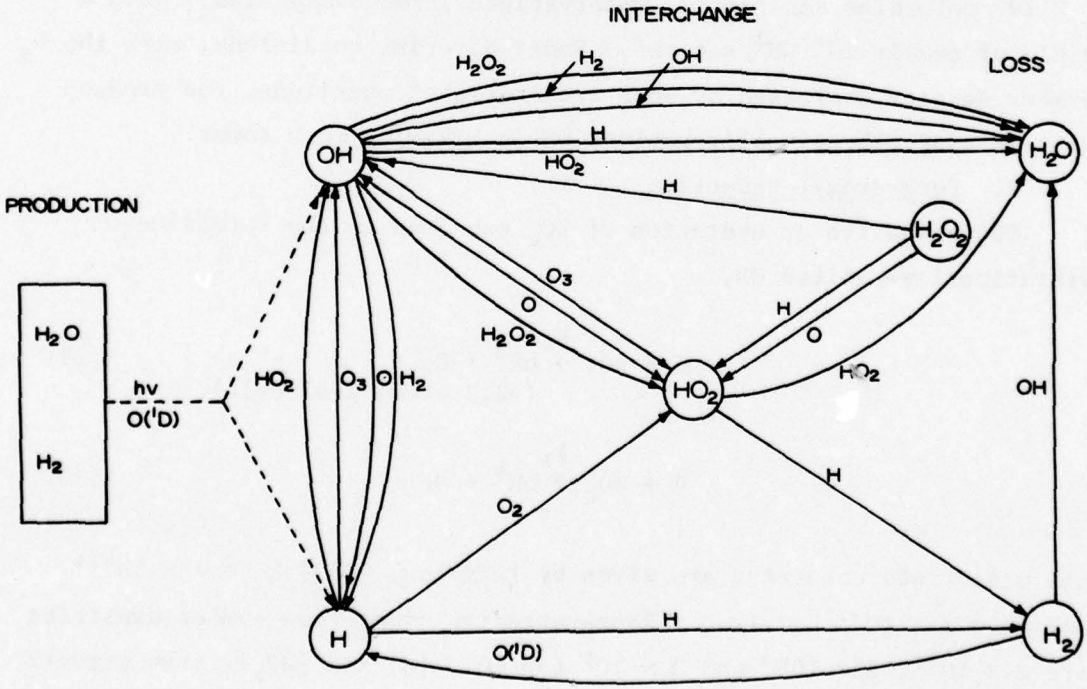

Figure 12. State diagram for atmospheric odd hydrogen.

C. Loss Mechanisms

When quasi-steady-state conditions obtain, the production of $OH^{\ddagger}$ is approximately balanced by the loss of vibrationally-excited OH. The two principal loss mechanisms are radiative relaxation and quenching. These photochemical reactions include the following:

$$OH^{\ddagger} \xrightarrow{k_4} OH^{\ddagger'} + h\nu \quad (k_4 = 10^2) \tag{31}$$

$$OH^{\ddagger} + O \xrightarrow{k_5} H + O_2 \quad (k_5 = 3 \times 10^{-12}\, T^{\frac{1}{2}}) \tag{32}$$

$$OH^{\ddagger} + M \xrightarrow{k_6} OH + M \quad (k_6 = 10^{-14}) \tag{33}$$

Representative number densities for [O] and [M] in the nighttime atmosphere at 85 km are 2×10^{11} and 5×10^{14} molecules/cm^3. Thus, quenching is often ignored in comparison with radiative relaxation in a first order modeling. The complete set of photochemical reactions, together with the appropriate rate constants, is given in Table 4.

The rate constants for interactions of $OH^{\ddagger}$ (v'=9) with M are given by *Worley et al*, [1972] in Table 4. As with O, the rate constants can be expected to be a function of v' and the resulting effects may be large if there exist near resonances between OH (v') energy level and an excited state of O or M. Such selective quenching, and possible pumping up of $OH^{\ddagger}$ by energy going the other way as well, could change the distribution of the OH state populations.*

As a first look, the loss rates for atmospheric OH at 85 km are calculated using representative day-night concentrations for the species involved. The results are tabulated in Table 5. By way of comparison (See Table 6) the production rate of $OH^{\ddagger}$ ($v \leq 9$) by the $H + O_3$ reaction ($k = 2.2 \times 10^{-11}$ cm^3 sec^{-1}) ranges from 2×10^3 mol. cm^{-3} sec^{-1} during the day to 4×10^4 at night using an atomic hydrogen concentration of 10^8 mol./cm^3 at 85 km. From Table 6 the radiative relaxation rate

---

*For example, the 15,868 cm^{-1} energy level of $OI(^1D)$ is close to the 16.201 cm^{-1} of $OH(X^2\Pi_{3/2}, v'=5)$.

Table 4. Rate constants for interactions of $OH^{\ddagger}$ (v'=9) with M [*Worley et al.*, 1972].

M	k cm^3 $molecule^{-1}$ sec^{-1}
O_3	$7.7 \pm 0.3 \times 10^{-12}$
O_2	$1.0 \pm 0.1 \times 10^{-14}$
N_2	$3.0 \pm 0.5 \times 10^{-15}$
NO	$1.5 \pm 0.3 \times 10^{-13}$
N_2O	$4.8 \pm 2.2 \times 10^{-14}$
CH_4	$1.4 \pm 0.2 \times 10^{-14}$
CO_2	$2.4 \pm 1.0 \times 10^{-14}$
COS	$2.5 \pm 1.5 \times 10^{-14}$
SO_2	$2.4 \pm 0.4 \times 10^{-14}$
H_2S	$2.5 \pm 0.9 \times 10^{-13}$
H_2O	$2.0 \pm 1.6 \times 10^{-13}$

Table 5. Loss rates of OH at 85 km.

M	[M] (cm^{-3}) Day - Night	k ($cm^3 sec^{-1}$)	k[M][OH] ($cm^{-3} sec^{-1}$) Day - Night
0	3×10^7 - 3×10^{11}	4.4×10^{-11}	1×10^1 - 1×10^6
N_2	10^{14}	3.0×10^{-15}	3×10^3 - 3×10^4
O_2	3×10^{13}	1.0×10^{-14}	3×10^3 - 3×10^4
O_3	10^6 - 10^7	7.7×10^{-12}	8×10^{-2} - 8×10^0

Night-day concentration of OH is taken as 10^4 - 10^5 cm^{-3}, respectively.

is on the order of 10^2 cm^3/sec for relaxation from the high (v>6) vibrational states and is about 30 for relaxation of the low states ($v \leq 6$) to the unexcited level.

A representative distribution might be 31% of the $OH^{\ddagger}$ at levels above v'=6 and the rest (69%) is at v'$\leq$6 (see Table 13). Consequently, the relaxation rate of $OH^{\ddagger}$ by radiation ranges from $E \times 10^6$ to $3E \times 10^6$ cm^{-3} sec^{-1}, where E is the ratio of the total OH which is in an excited $X^2\Pi_i$ state. Thus, it appears that at 85 km the radiative relaxation dominates the quenching by collision processes given in Table 5.

D. Vibrational Distributions

Unlike the rotational levels, the thermal distribution of the vibrational levels can be expressed as a simple Maxwell-Boltzmann factor $e^{-E/kT}$. The number of molecules in the state v is

$$N_v = \frac{N}{Q_v} e^{-G_o(v)hc/kT} \tag{34}$$

where N is the total number of molecules, Q_v is the partition function, and $G_o(v)$ is the vibrational energy term value referred to the lowest level,

$$G_o(v) = \omega_o v - \omega_o x_o v^2 + ... \tag{35}$$

where $\omega_o = \omega_e - \omega_e x_e + ...$ and $\omega_o x_o = \omega_e x_e - . . . .$

For the $OH(X^2\Pi_i)$ molecule the parameter values [*Kifte*, 1959] are ω_o = 3,651 cm^{-1} and $\omega_o x_o$ = 82 cm^{-1}. The values of $G_o(v)$ for OH are given in Table 7.

The entity $R_{v',v''}/\sigma^3_{v',v''}$ is called the vibrational band strength (analogous to the rotational line strength S_J). The sum of the band strengths of all bands with the same upper state is proportional to the number of molecules $N_{v'}$ in the upper state

$$\sum_{v''} R_{v',v''}/\sigma^3_{v',v''} \propto N_{v'} \tag{36}$$

since the dipole-moment overlap integral evaluates to a constant when squared and summed over all v". Since in thermal equilibrium the population $N_{v'}$ is proportional to $\exp[-G_o(v')hc/kT]$, we can substitute Equation (36) into (34) to obtain

Table 6. OH atmospheric photochemical reaction set [*Moore* and *Kennealy*, 1975].

No.	Reactions	Rate coefficients (cm^3/sec)	Reference
1	$O + O_2 + M \rightarrow O_3 + M$	$k = 1.05\ exp(-34)\ exp(520/T)$	Davis, 1972
2	$O + O_3 \rightarrow O_2 + O_2$	$k = 2.05\ exp(-11)\ exp(-215/T)$	McCrumb, 1972
3	$O + O + M \rightarrow O_2 + M$	$k = 3.6\ exp(-31)\ T^{-1}\ exp(-170/T)$	Schiff, 1969
4	$O + OH \rightarrow H + O_2$	$k = 3.0\ exp(-12)\ T^{.5}$	Nicolet, 1972
5	$O + H_2O_2 \rightarrow OH + HO_2$	$k = 1.0\ exp(-15)$	Foner, 1962
6	$O + OH + M \rightarrow HO_2 + M$	$k = 1.4\ exp(-31)$	Hunt, 1966
7	$O(^1D) + M \rightarrow O + M$	$k = 5.47\ exp(-11)$	NBS, 1973
8	$O(^1D) + H_2 \rightarrow OH + H$	$k = 1.9\ exp(-10)$	Young, 1968
9	$O(^1D) + O_3 \rightarrow O_2 + O_2$	$k = 5.0\ exp(-10)$	NBS, 1973
10	$O(^1D) + H_2O \rightarrow OH + OH$	$k = 3.5\ exp(-10)$	NBS, 1973
11	$O(^1D) + O_2 \rightarrow O + O_2(^1\Sigma)$	$k = 7.45\ exp(-11)$	NBS, 1973
12	$O_2(^1\Sigma) + M \rightarrow O_2 + M$	$k = 1.5\ exp(-15)$	Noxon, 1970
13	$O_2(^1\Sigma) \rightarrow O_2$	$k = 8.5\ exp(-02)$	Noxon, 1970
14	$O_2(^1\Delta) + M \rightarrow O_2 + M$	$k = 2.5\ exp(-20)\ T^{.5}$	Findlay, 1969
15	$O_2(^1\Delta) \rightarrow O_2$	$k = 2.6\ exp(-04)$	Badger, 1965
16	$H + O_2 + M \rightarrow HO_2 + M$	$k = 3.3\ exp(-33)\ exp(800/T)$	Nicolet, 1972
17	$H + H + M \rightarrow H_2 + M$	$k = 6.1\ exp(-31)\ T^{-.7}$	Kaufman, 1969
18	$OH + M \rightarrow H_2O + M$	$k = 2.5\ exp(-31)$	Kaufman, 1964
19	$H + HO_2 \rightarrow H_2 + O_2$	$k = 2.0\ exp(-13)$	Clyne, 1963

Table 6. Continued.

No.	Reactions			Rate coefficients (cm^3/sec)	Reference
20	$H + H_2O_2$	→	$H_2 + HO_2$	k = 1.0 exp(-13)	Foner, 1962
21	OH + OH	→	$H_2O + O$	k = 7.5 exp(-13) $T^{.5}$ exp(-500/T)	Nicolet, 1972
22	$OH + O_3$	→	$HO_2 + O_2$	k = 1.5 exp(-13) $T^{.5}$ exp(-3000/T)	Nicolet, 1972
23	$OH + H_2$	→	$H_2O + H$	k = 2.0 exp(-13) $T^{.5}$ exp(-1800/T)	Nicolet, 1972
24	$OH + H\dot{O}_2$	→	$H_2O + O_2$	k = 2.0 exp(-10)	Hochanadel, 1972
25	$OH + H_2O_2$	→	$H_2O + HO_2$	k = 4.1 exp(-13) $T^{.5}$ exp(-600/T)	Greiner, 1968
26	$HO_2 + HO_2$	→	$H_2O_2 + O_2$	k = 9.5 exp(-12)	Hochanadel, 1972
27	$HO_2 + O_3$	→	$OH + O_2 + O_2$	k = 1.0 exp(-14)	Hunt, 1966
28	$H + O_3$	→	OH VH + O_2	k = 1.5 exp(-12) $T^{.5}$	Nicolet, 1972
29	$H + HO_2$	→	OH + OH VL	k = 3.0 exp(-12)	Kaufman, 1969
30	$O + HO_2$	→	OH VL + O_2	k = 2.0 exp(-11)	Kaufman, 1969
31	OH VH	→	OH VL	k = 1.0 exp(02)	Moore, 1973
32	OH VH + OH	→	OH VL + OH VL	k = 1.0 exp(-11)	Moore, 1973
33	OH VL	→	OH	k = 3.0 exp(01)	Moore, 1973
34	OH VL + M	→	OH + M	k = 1.0 exp(-14)	Moore, 1973
				Max Cross Section (cm^2/mol)	
35	$O_2 + h\nu$	→	$O + O(^1D)$	1.5 exp(-17)	
36	$O_2 + h\nu$	→	O + O	2.5 exp(-19)	

Table 6. Continued.

No.	Reactions	Max Cross Section (cm^2/mol)	Reference
37	$O_2 + h\nu \rightarrow O + O$	1.2 exp(-23)	
38	$O_3 + h\nu \rightarrow O(^1D) + O_2(^1\Sigma)$	1.1 exp(-17)	
39	$O_3 + h\nu \rightarrow O(^1D) + O_2(^1\Delta)$	8.0 exp(-18)	
40	$O_3 + h\nu \rightarrow O_2 + O$	4.3 exp(-20)	
41	$H_2O + h\nu \rightarrow OH + H$	2.0 exp(-17)	

Table 7. Vibrational term values for $X^2\Pi$ state of OH.

v'	$G_o(v)$ (cm^{-1})	
	$\Omega = 3/2$	$\Omega = 1/2$
0	0	126.3
1	3,568.4	3,695.2
2	6,971.1	7,097.3
3	10,210.5	10,336.6
4	13,287.0	13,415.7
5	16,201.0	16,330.3
6	18,952.1	19,082.1
7	21,538.0	21,671.3
8	23,949.4	24,080.1
9	26,184.3	26,316.4

Table 8. Thermally-averaged $OH(X^2\Pi_i)$ vibrational Einstein coefficients $A_{v'v''}(sec^{-1})$ for 200°K [*Mies*, 1974].

v' (from) / v'' (to)	9	8	7	6	5	4	3	2	1
8	50.65								
7	146.6	25.84							
6	90.28	166.8	9.142						
5	10.81	60.84	163.4	2.347					
4	1.189	5.67	37.32	141.5	4.47				
3	0.130	0.569	2.907	20.99	108.4	12.25			
2		.030	0.183	1.274	10.62	72.61	20.90		
1				.053	0.392	4.29	39.93	25.24	
0					.050	.079	0.920	14.07	20.15
TOTALS	299.7	259.8	213.0	166.3	124.0	89.23	61.75	39.31	20.15

$$\ln \sum_{v'} \frac{R_{v'v''}}{\sigma^3_{v'v''}} = C_1 - \frac{G_o(v')hc}{kT} \qquad (37)$$

where C_1 is a constant.

Therefore, by plotting the logarithms of the band strength sums $\Sigma[R_{v',v''}/\sigma^3_{v',v''}]$ versus the vibrational term values $[G_o(v')]$, a straight line is obtained whose slope* is hc/kT and thus gives the vibrational temperature T. The band strengths need only be relative. Unless conditions of thermodynamic equilibrium exist, the vibrational temperature will not necessarily equal the rotational temperature. Even for non-thermal conditions, the plot will often approximate a straight line (by a least squares fit) to give an apparent vibrational temperature.

The relative populations observed in sequences of the OH airglow are the net result of a number of factors: (1) the population upon formation by one or more photochemical mechanisms, (2) subsequent cascading with level-dependent lifetimes, and (3) quenching with possible energy selectivity (resonances). Since these factors depend upon the concentrations and temperature, a complete modeling is required taking into account the diurnal variations of solar energy and its depth of penetration.

The $H + O_3 \rightarrow OH^{\ddagger} + O_2$ reaction has just enough exothermic energy (heat of formation) to vibrationally excite the OH up through the 9th level.

$$\sigma = \frac{1}{\lambda} = \frac{f}{c} = \frac{eV}{hc} \qquad (38)$$

$$= \frac{1.60 \times 10^{-19}(3.3)}{6.63 \times 10^{-34}(3.0 \times 10^{10})} = 26{,}500 \text{ cm}^{-1}$$

as can be seen from Table 7. The energy level for v = 9 is 26,184 cm^{-1}. The $H + HO_2$ reaction, on the other hand, has an exothermic energy of only 2.3 eV = 18,500 cm^{-1}. Consequently, the chief perhydroxyl mechanism excites vibrational levels $v \leq 6$, where translational energy is available.

---

*The numerical value of hc/k is 1.439 °K/cm^{-1}.

Upon formation of $OH^{\ddagger}$ by the hydrogen ozone reaction, the v = 9 and 8 states apparently receive most of the energy. *Polanyi* [1971] gives the initial formation distribution of Table 9.

Table 9. Relative vibrational level populations of OH ($X^2\Pi_i$) formed by $H + O_3$ in terms of percentages [*Polanyi* 1971].

				6 thru 0
v'	9	8	7	
$N_{v'}$	$\geq$38%	$\geq$31%	$\leq$15%	$\leq$15%

The vibration levels below v = 9 are significantly populated by cascading from v = 9 and 8. The branching ratios are obtained from the transition probabilities. Table 10 summarizes these in terms of percentages.

Table 11 gives the results of a computation of the steady-state relative emission radiances of the vibration bands of $OH(X^2\Pi_i)$. These theoretical intensities were computed ignoring any quenching or collision effects. A steady-state condition was assumed using an initial formation ratio of 46.8%:38.2%:15%, respectively, into the v = 9, 8 and 7 levels. The branching ratios of Table 8 were used. The results are expressed as percentages of the formation rate of OH from the $H + O_3$ reaction.

The theoretical relative band radiances of Table 11 and the band origin wavenumbers of Table 12 were used in Equation (37) to calculate the relative populations of the vibrational levels. The results are tabulated in Table 11. It is evident that a straight line fit of $\ln\Sigma R_{v'v''}/\sigma^3_{v'v''}$ to G(v') does not occur over all the values of v'. The distribution is non-Boltzmann as to be expected since thermal equilibrium conditions have not been imposed. It is interesting to note, though, that a nearly straight line does occur for $v' \leq 5$. A least squares fit gives a slope of T = 9500°K.

Table 10. Branching ratio percentages for $OH^{\ddagger}(X^2\Pi_1)$ cascading.

v' (from) / v'' (to)	9	8	7	6	5	4	3	2	1
8	16.9								
7	48.9	9.9							
6	30.1	64.2	4.3						
5	3.6	23.4	76.7	1.4					
4	0.4	2.2	17.5	85.1	3.6				
3		0.2	1.4	12.6	87.4	13.7			
2				0.8	8.6	81.4	33.8		
1					0.3	4.8	64.7	64.2	
0							1.5	35.8	100

Calculated from Einstein coefficients of *Mies* [1974] for 200°K.

In those situations where quenching is important (daytime, lower altitude $OH^{\ddagger}$), the vibrational distributions will, of course, be altered. The general effect can be expected to show up as a decreased population of the lower vibrational levels relative to the upper. This is because quenching would tend to occur before the time-consuming cascading process could be carried out.

The effect on the vibrational level populations of inclusion of the perhydroxyl reactions, on the other hand, would be to populate low v levels relative to the high. This is because of the lower exothermicity of the HO_2 reactions relative to the O_3.

Table 11. Relative emission band intensities of steady-state, unquenched $OH(X^2\Pi_i)$ from $H + O_3$.

v' (from) / v'' (to)	9	8	7	6	5	4	3	2	1
8	8%								
7	23	5							
6	14	30	2						
5	2	11	33	1					
4		1	7	39	2				
3			1	6	40	6			
2					4	40	18		
1						2	34	40	
0							1	22	76

Calculated using formation populations of *Polanyi* [1971] and transition probabilities of *Mies* [1974] for 200°K, and expressed as a percentage of total formation rate of OH.

Table 12. Wavenumbers (cm^{-1}) for $OH(X^2\Pi_i)$ vibrational band origins.

v' (from) / v'' (to)	9	8	7	6	5	4	3	2	1
8	2236								
7	4650	2414							
6	7236	4999	2585						
5	9987	7751	5336	2752					
4		10666	8252	5667	2915				
3			11329	8744	5993	3078			
2					9233	6318	3240		
1						9722	6644	3404	
0							10212	6974	3570

Table 13. Theoretical relative $OH(X^2\Pi_i)$ vibrational population distribution.

v'	9	8	7	6	5	4	3	2	1
$N_{v'}$	16%	10	5	4	4	6	10	17	27
G(v) (cm^{-1})	26,184	23,949	21,538	18,952	16,201	13,287	10,210	6,971	3,568

Calculated from theoretical radiance distribution (Table 9) without quenching.

VII. $OH^{\ddagger}$ AERONOMY

A. Altitude Distributions

Although a number of ground-based techniques have been attempted over the years, at present there are only two satisfactory methods of ascertaining the distribution of OH airglow emissions with altitude:

1. Flying a rocket with an onboard sensor through the layer.
2. Obtaining an exo-atmospheric limb look at the layer from a sensor onboard a rocket or satellite.

The latter approach has the advantage of higher signal levels, more nearly simultaneous observation of the portions of the profile, observation of lateral spatial variations, and longer observing times of the layer. The disadvantages are a more complicated geometry, possible long path absorption or stimulated emission effects, and the need for very narrow fields of view (at least in one dimension) with extremely good out-of-field rejection.

Most measurements of OH emission altitude profiles available to date have been obtained from vertically-viewing sensors flown aboard rockets. The technique has been well described by *Packer [1961]*. A composite of such measurements is given in Figure 13. These measurements, which were made in the visible region were complicated by a background continuum as well as the usual problem of unfolding the aspect geometry [see *Grieder et al.*, 1976].

In the AFGL/USU program, infrared rather than visible-range sensors were used to alleviate the background continuum problem. (The continuum has a different altitude distribution than the $OH^{\ddagger}$.) The sensors, developed in the USU Electro-Dynamics Laboratories (EDL) by Wyatt, Kemp and Frodsham, are dual-channel radiometers. Filters were selected (Figure 14) to obtain simultaneous measurements of the zenith radiance in two separate wavelength intervals. This makes it possible to look for a different altitude distribution for $OH^{\ddagger}(\Delta v<6)$ than for the $OH^{\ddagger}(\Delta v>6)$.

The 4720 to 5400-cm^{-1} (1.85-2.12 μm) bandpass includes the (8,6) and (7,5) emission bands of OH, and the 5820 to 6075-cm^{-1} (1.64-1.72 μm^{-1}) bandpass includes the OH (5,3) band. A second filter of bandpass

5960 to 6820 cm^{-1} (1.47-1.68 μm) has also been employed on some flights. In order to obtain the OH band intensity distribution, it is desirable to look at only one band per channel. However, this simplification is achieved at the cost of signal-to-noise ratio.

In Figure 15 the volume emission rate profiles from four different flights from the AFGL/USU program are presented [*Ulwick* and *Grieder*, 1975, and *Rogers et al.*, 1973]. Two of the profiles were made under night conditions at the U.S. Army's White Sands Missile Range (WSMR) in New Mexico. The other two profiles were obtained at the University of Alaska's Poker Flat Research Range (PFRR) in Alaska. One was taken during the night and the other at evening twilight. In both latter cases, although the measurements were taken in the auroral zone, quiet conditions prevailed at the time. In Figure 16 the profiles of the $OH^{\ddagger}$ ($v < 6$) band measurements of three of the flights are given as indicated.

To facilitate the comparison, all six profiles are plotted on the same scale in Figure 17. The apparent emission layer centers and depths from each measurement are summarized in Table 14. From these data the layers appear as Chapman-like with a usual half-intensity depth of about 8 km. It would also appear that the centers (between half intensity points) lie between 84 and 89 km in altitude.

There is evidence that during evening twilight ($\chi = 80°$ in this case) that the layer is formed at a slightly lower altitude than is the case at night-time ($\chi = 116°$). However, the twilight signal-to-noise ratios of the measurement are much lower than during the daytime (Figure 15), and so at best the altitude resolution of the volume emission rate profile is several kilometers. The volume emission rate η is computed from the zenith radiance profile using [*Baker*, 1974]

$$\eta = 10 \frac{dR}{dh} \text{ (photons sec}^{-1} \text{ cm}^{-3}\text{)} \qquad (39)$$

where R is in rayleighs [megaphotons sec^{-1} $(cm^2 \text{ column})^{-1}$] and the altitude h is in km. The signal-to-noise ratio and therefore the altitude resolution of the slope dR/dh of the profile is much lower than that of the zenith radiance profile itself.

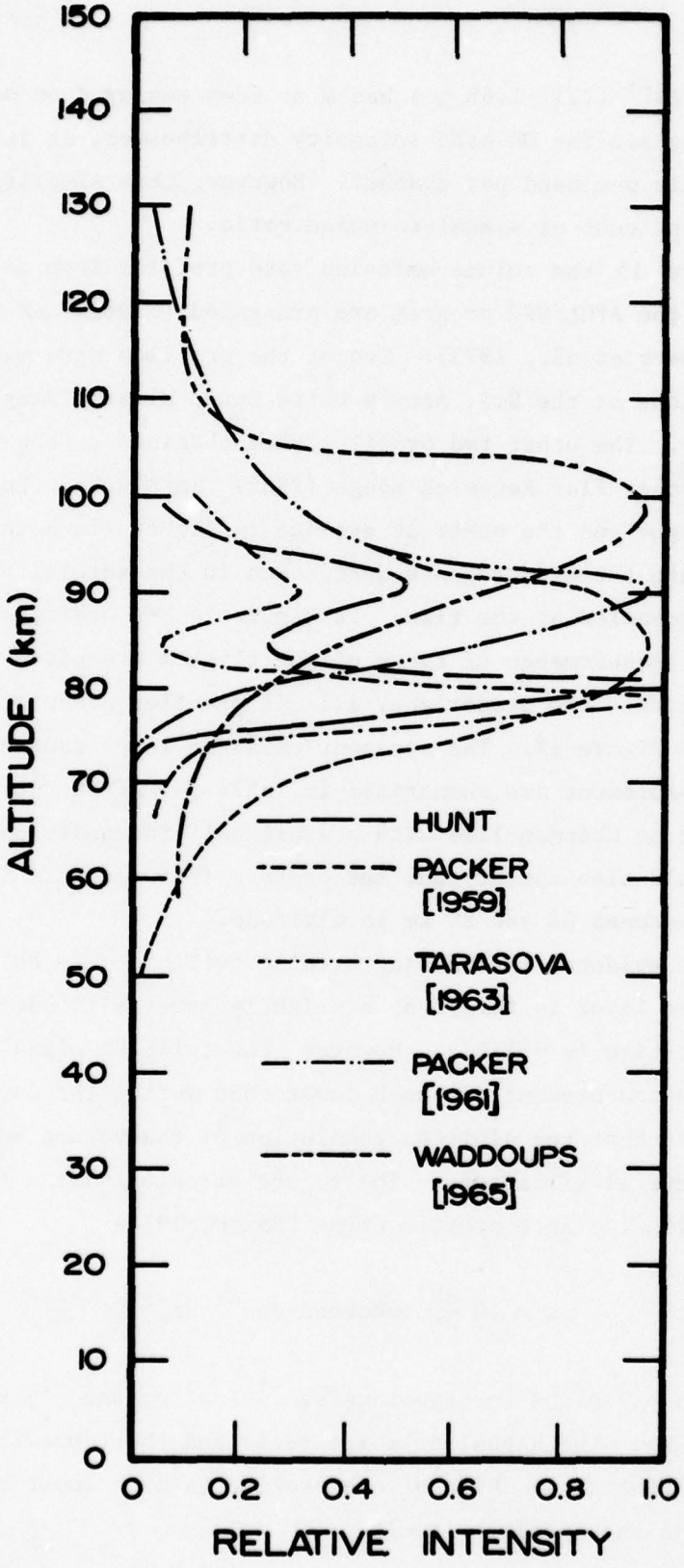

Figure 13. Altitude profiles of the night-sky airglow OH emission.

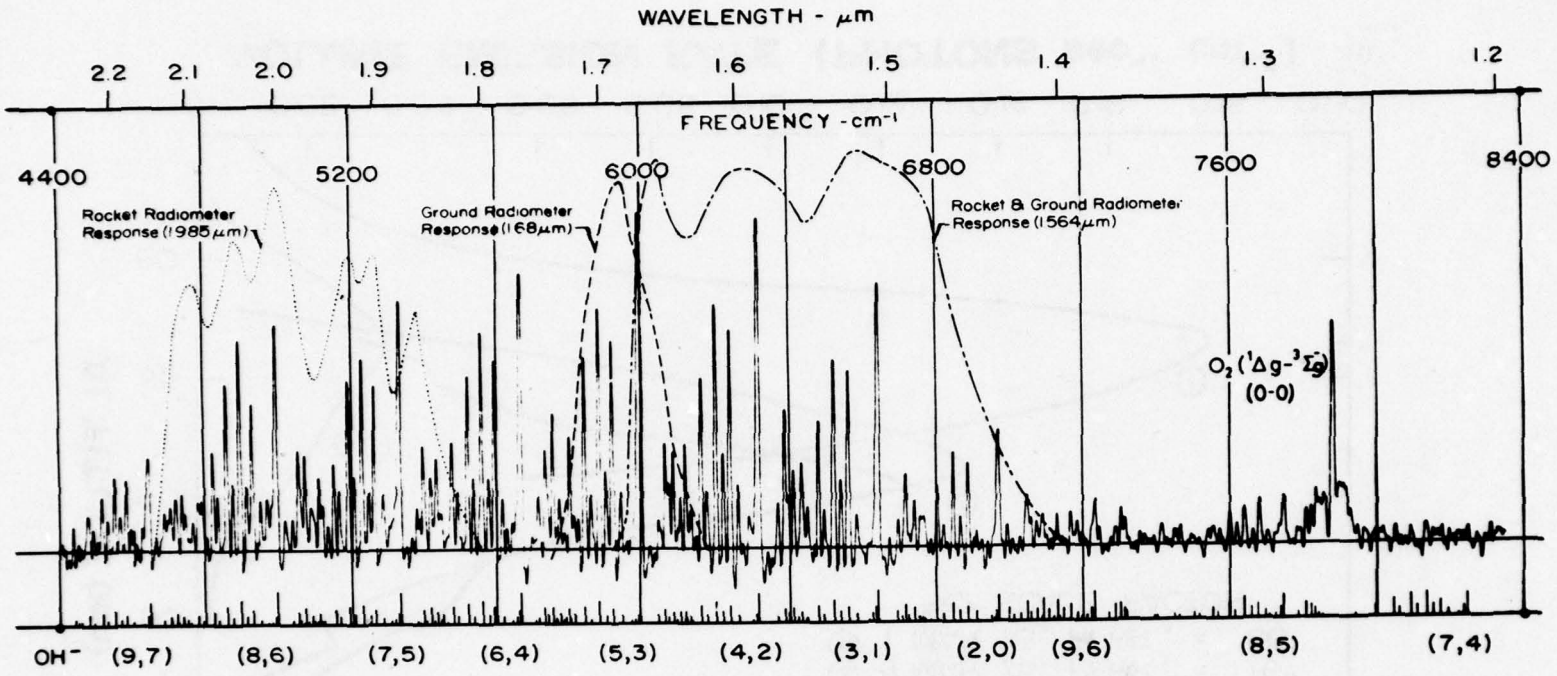

Figure 14. Radiometer filter coverage of OH ($\Delta v=2$) sequence superimposed on *Gush et al.* balloon-borne spectrum.

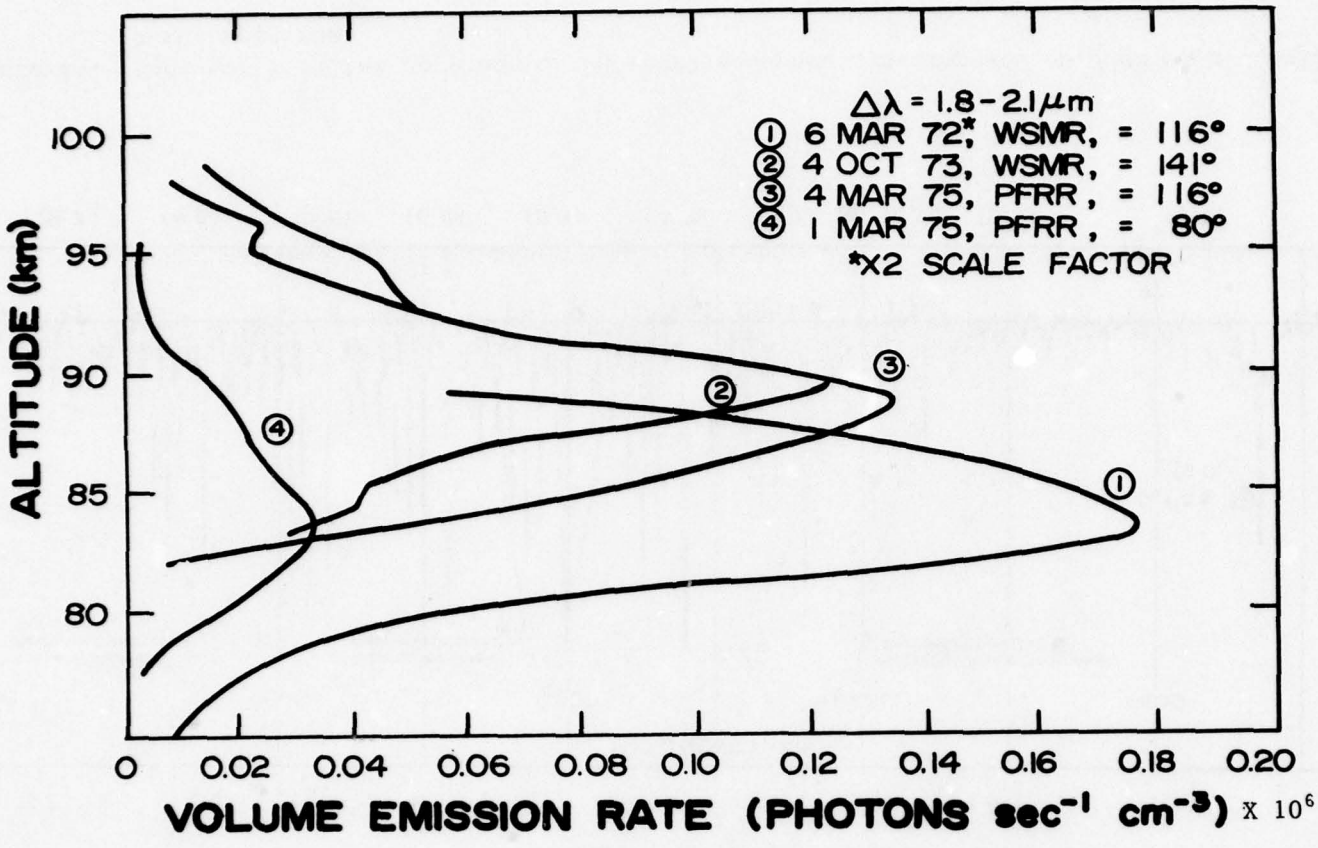

Figure 15. OH (v>6) airglow emission profiles.

Murphy suggested that the OH volume emission rate profile, computed from the slope of the measured zenith radiance versus altitude curve, can in turn be used to calculate the altitude profile of atomic oxygen concentration. This technique was carried out by *Rogers et al.* [1973] and *Good* [1976]. The formula, ignoring deactivation processes other than radiative relaxation, is

$$[O] = \frac{10\ dR/dh}{\varepsilon p k [O_2][M]} \quad (cm^{-3}) \tag{40}$$

where R is the zenith radiance in the radiometer filter bandpass, ε is the ratio of the radiance in the bandpass to the total radiance from $OH^{\ddagger}$ at all wavelengths, p = 3.9 is the production efficiency (number of photons emitted per OH molecule formed), $k = 1.1 \times 10^{-34} \exp(500/T)$ $cm^{-6} sec^{-1}$ is the reaction rate for the formation of ozone by $O + O_2 + M \rightarrow O_3 + M$ and $[O_2]$, $[M]$ are the concentrations of molecular oxygen and the total atmosphere (primarily N_2), respectively.

B. Spatial Distributions

The horizontal spatial distribution of the upper atmospheric OH airglow emission layer can be observed from flying aircraft, from a network of surface-based sensors or from one or more sensors which can scan in elevation and azimuth. The latter technique requires corrections for the Van Rhijn effect in looking obliquely at an extended, optically-thin emitting layer.

Kieffaber [1973] has used the latter technique to carefully make an extensive set of OH sky emission contours. A pronounced latitudinal gradient decreasing from north to south in the Northern Hemisphere has been observed. Also, by using image intensifiers *Peterson and Kieffaber* [1974] have observed apparent emission cells and patchiness.

Both the latitudinal gradient and the apparent patchiness of the OH atmospheric airglow have been observed using infrared filter radiometers aboard the AFGL KC-135 flying laboratory. The decrease of OH(5,3) band radiance with latitude is illustrated in Figure 18. The cellular phenomena are illustrated in Figure 19. The lateral extent of a cell ranges perhaps from ten to as much as a hundred miles.

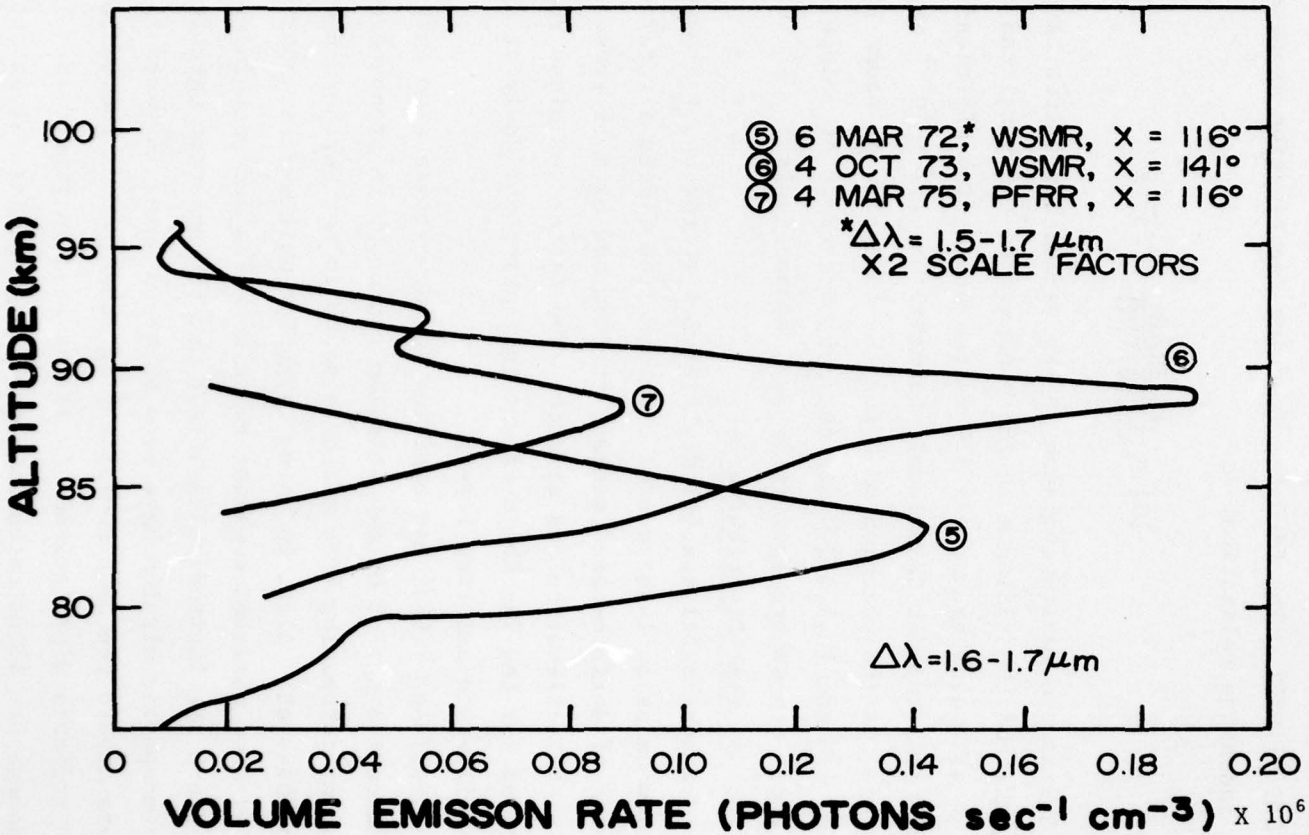

Figure 16. OH (v<6) airglow emission profiles.

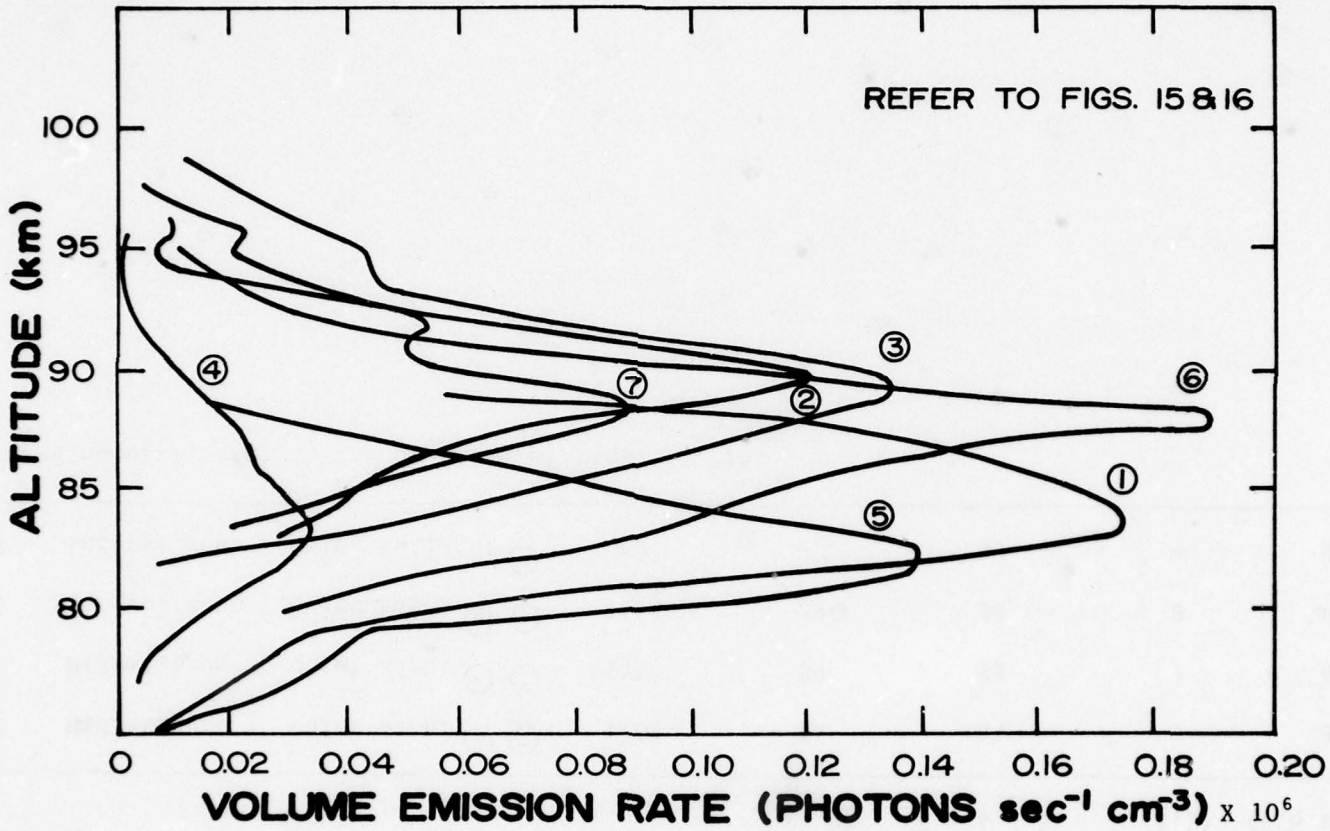

Figure 17. Composite of AFGL/USU OH emission profiles.

Table 14. AFGL/USU rocketborne measurements of OH airglow emission layers.

Date	Location	Conditions*	Solar Zenith Angle ψ [deg]	Layer Center Altitude h_m [km]		Layer Depth Δh [km]	
				(5,3)	(8,6 & 7,5)	(5,3)	(8,6 & 7,5)
6 Mar 72	Midlatitude	Quiet Night ⑤,①	116°	84	85	7	8
4 Oct 73	Midlatitude	Quiet Night ⑥,②	141°	89	89	7	6
4 Mar 75	Auroral zone	Quiet Night ⑦,③	116°	89	88	8	8
1 Mar 75	Auroral zone	Quiet Twilight ④	80°	-	85	-	9

*The circled numbers refer to the profiles of Figs. 15, 16.

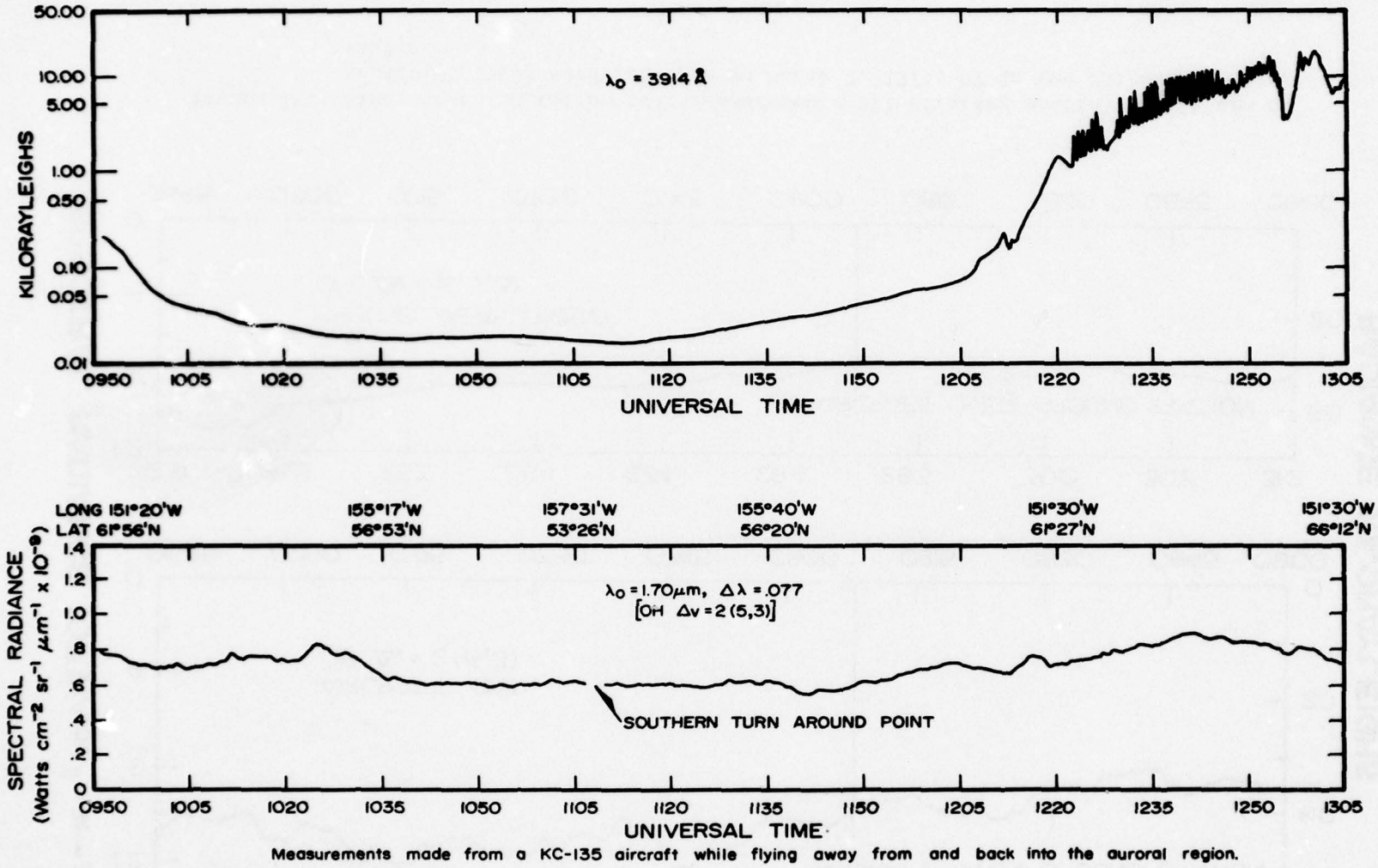

Figure 18. Measurements of zenith OH (5,3) band radiance made from KC-135 aircraft while flying away from and back into the auroral region on March 15, 1975.

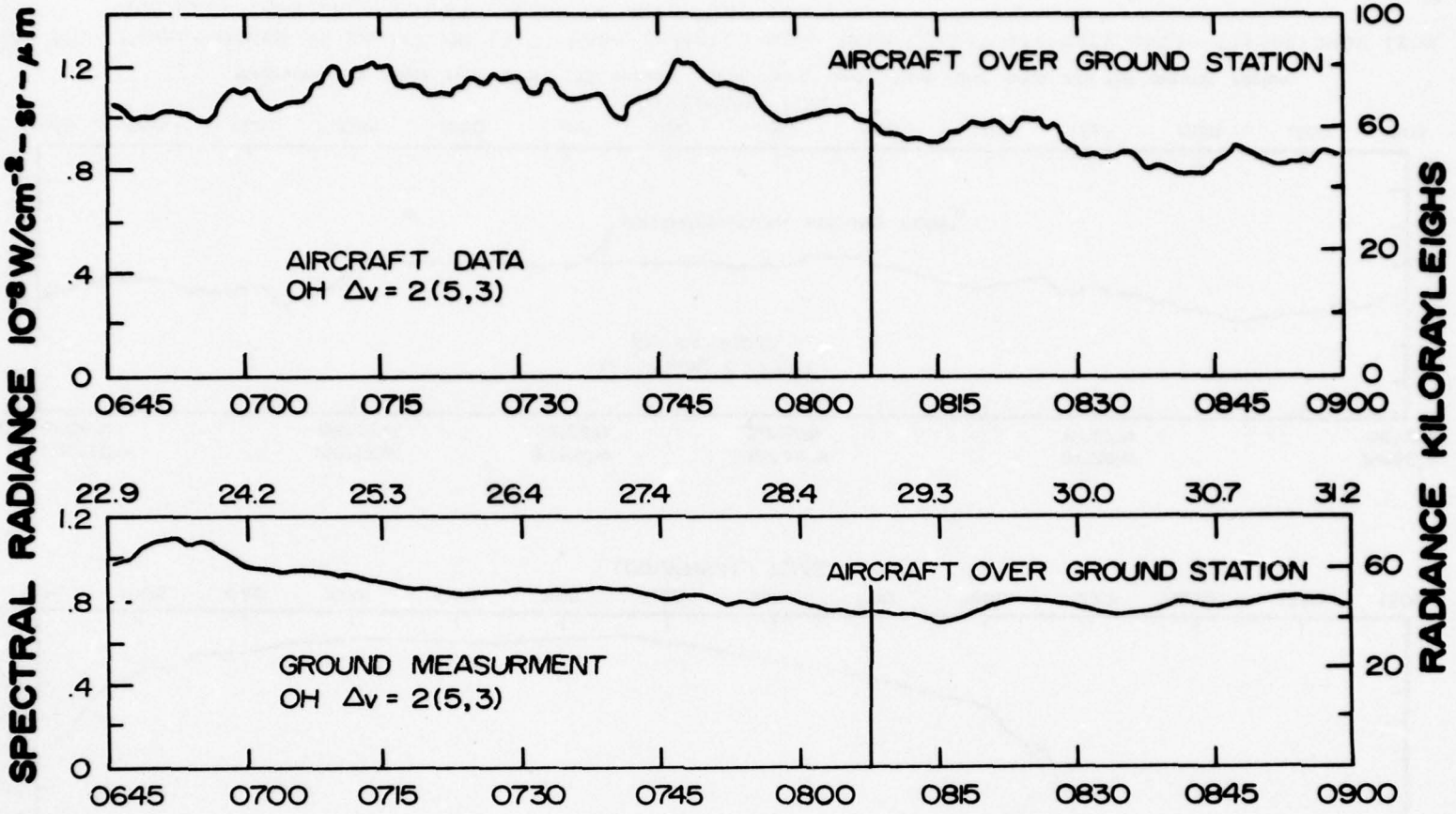

Figure 19. Aircraft-borne radiometric measurements illustrating spatial variations of zenith OH (5,3) band radiance on March 2, 1975, UT in the Fairbanks, Alaska region.

C. Dynamical Behavior

The temporal variations of the atmospheric OH airglow can be categorized as follows: An attempt to generalize these temporal changes is made in Table 15.

Table 15. Temporal variation generalization of OH airglow.

Period of Variation	Categorization	Characterization
Minutes	High-frequency fluctuations	Appears as high variance on radiance and rotational temperature measurements.
Hours	Low-frequency fluctuations	Appears as wave-like modulation of slowly-changing radiance and temperature levels.
Daily	Diurnal variations	Cyclical changes of OH levels with two twilights as the transition between day-time and night-time conditions.
Monthly	Periodical variations	Appears as slowly changing radiances and temperatures from night to night in auroral zone associated with solar rotation.
Yearly	Seasonal changes	Appears as brighter radiance in winter than summer.
Decade	Epochal changes	Would appear as changes with the solar cycle.

With the advent of spectrometers of high throughput and detectors of high (signal-to-noise) sensitivity, it is possible to observe successive spectra of the OH bands taken tens of seconds apart. Unexpectedly, the

rotational temperatures calculated from the successive spectra exhibit a variance of about five degrees (Kelvin). This may be a noise artifact of the instrumentation, or it may be characteristic of a "granular" OH layer. The temperature "seen" is an integrated effect over some 8 kilometers in a dynamic, optically-thin medium.

The longer term fluctuations are illustrated in Figure 20. Both the radiance of the OH(5,3) band and its rotational temperature appear to fluctuate with a not consistently repeating period of about an hour. *Merriwether* [1974], *Shefov* [1970] and others have reported seeing similar patterns of fluctuations. *Armstrong* [1976] theorizes that these fluctuations are due to acoustical gravity waves. Perhaps they are associated with the deposition of energy in the auroral regions. The changes of intensity and of rotational temperatures might be due to the vertical displacement of the emission layer. The reaction rates are temperature dependent; the temperature asymptote toward which the rotational states of the OH molecules tend to equilibrate is dependent upon altitude. If the low frequency fluctuations are due to wavemotions, the speed at which the waves are propagated is of interest. Krassovsky reports: "After geomagnetic storms an enhanced hydroxyl emission domain moves from high latitudes towards the equator at a speed of about 10^3 cm/sec."

Establishing the intensity levels and rotation-vibrational distributions of the OH airglow as it undergoes diurnal variations is of high priority. Lytle [*Hunten*, 1967] made an early measurement of the sharp fall of hydroxyl emission intensity at the moment of morning-time illumination of the atmosphere at 80 km. *Moreels* [1970] has reported similar balloon-borne measurements. More extensive measurements of the diurnal variations have been made [*Huppi and Stair*, 1969] from aboard the AFGL aircraft. Typical ground-based measurements of the night-time variation of OH(5,3) band emission at Poker Flat and at White Sands are shown in Figure 23 and Figure 24. The *Moore-Kennealy* [1975] atmospheric computer program is particularly suited for applying changing solar radiation onto a distributed chemical model of the upper atmosphere. Their predicted diurnal variation of the OH concentration at 80 and 90 km

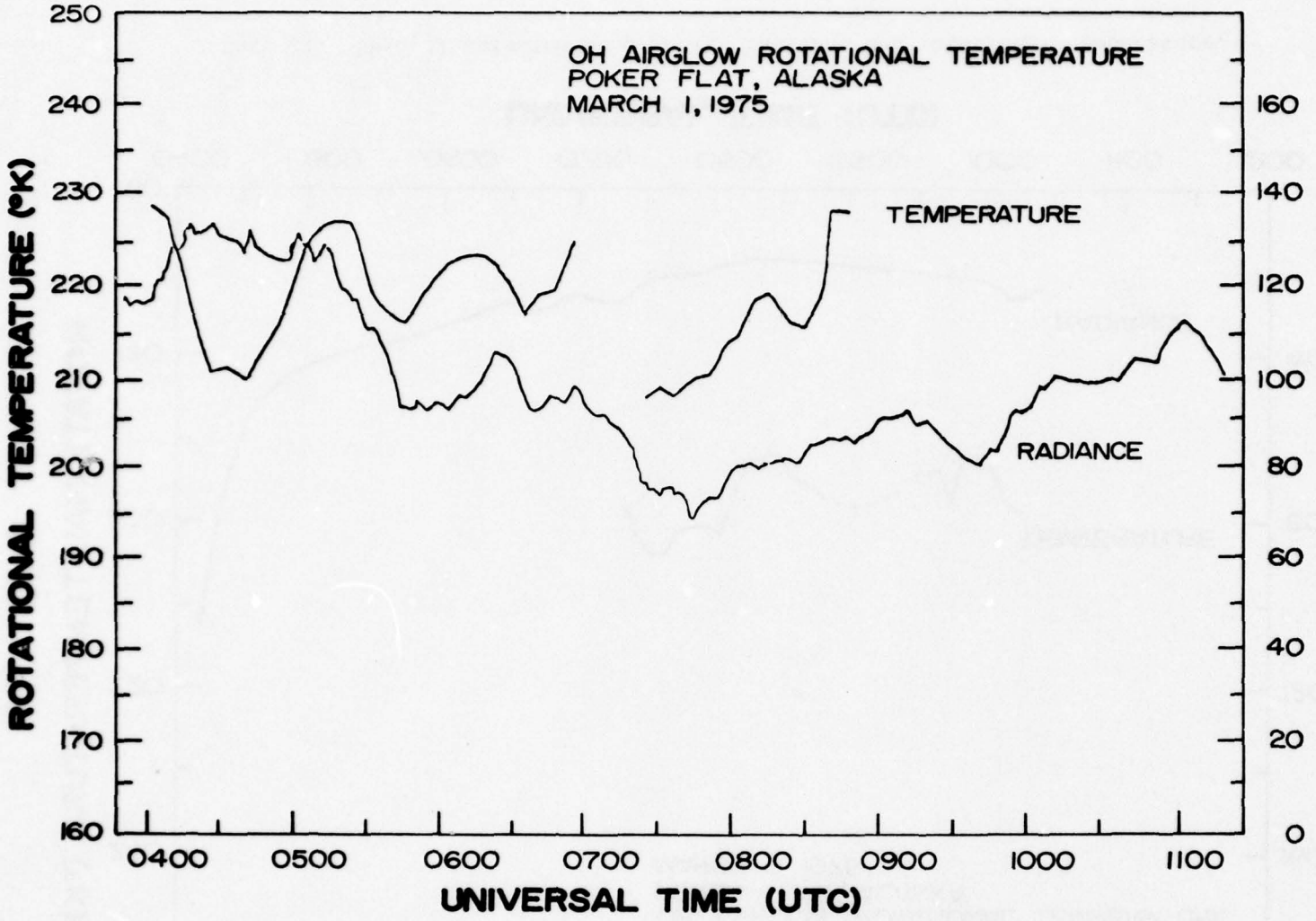

Figure 20. OH(5,3) emission band zenith radiance and rotational temperature.

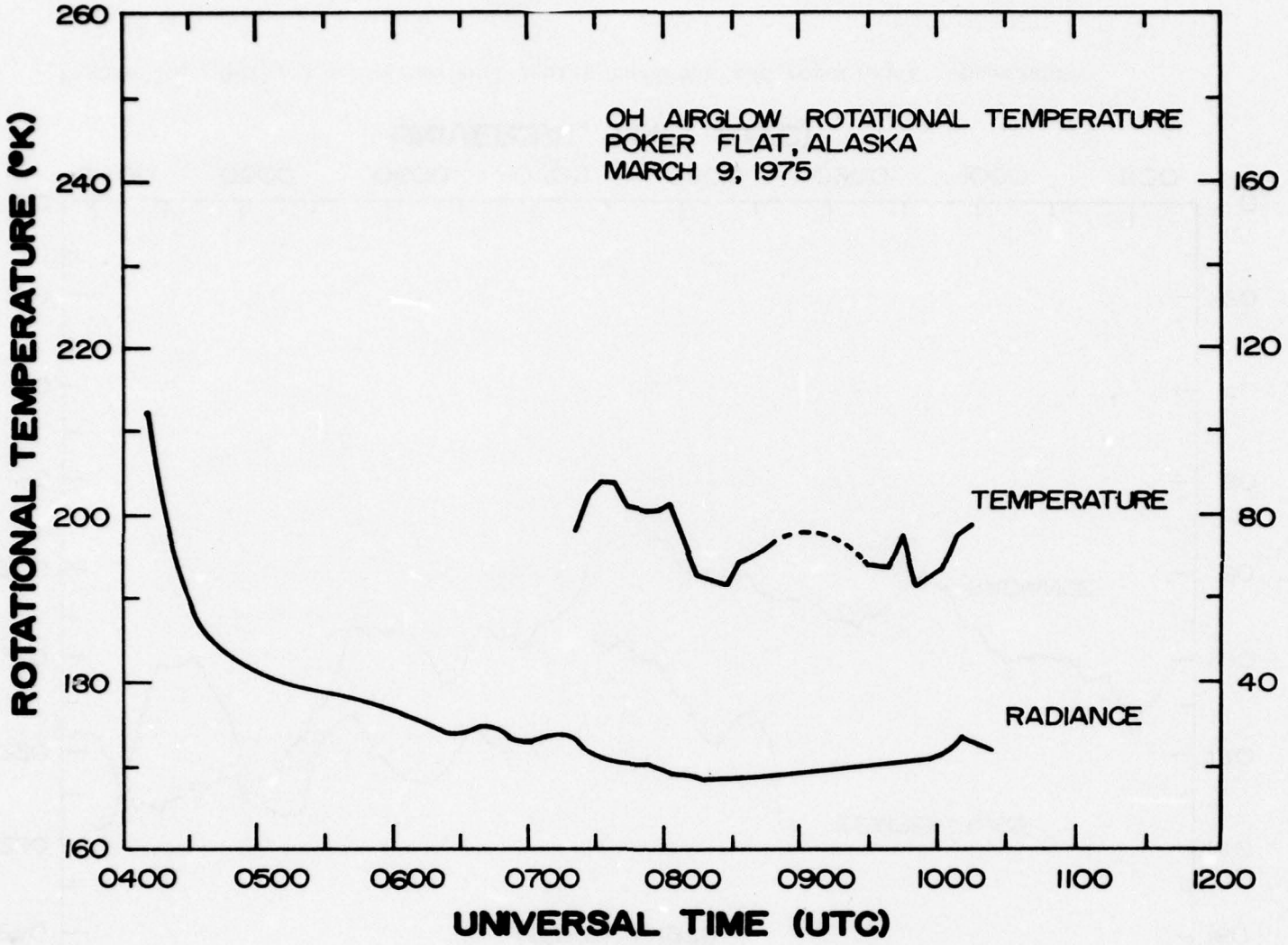

Figure 21. OH(5,3) emission band zenith radiance and rotational temperature.

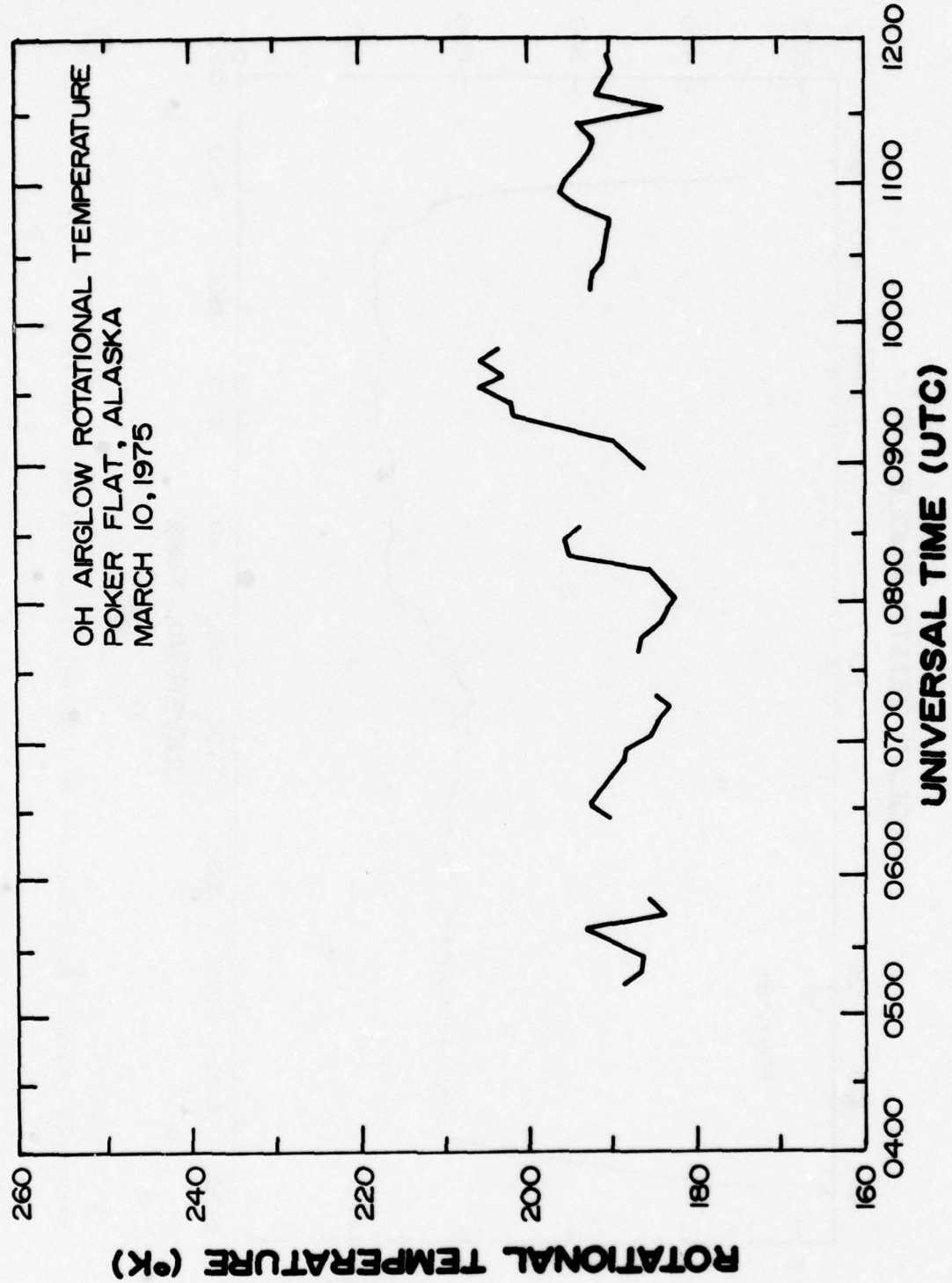

Figure 22. OH(5,3) emission band zenith rotational temperature.

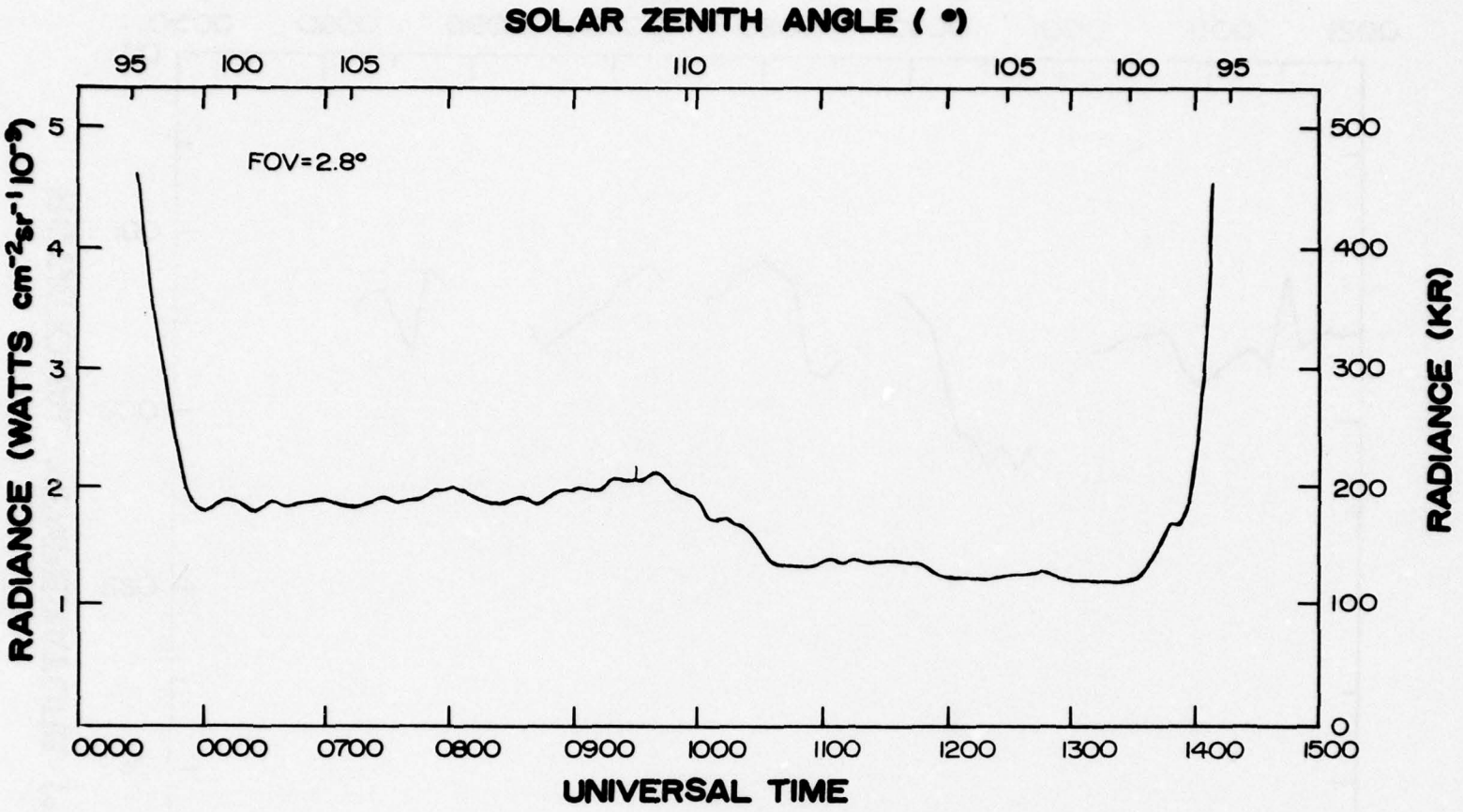

Figure 23. Zenith radiance 1.47 to 1.48 μm, Poker Flat on 2 Apr 73.

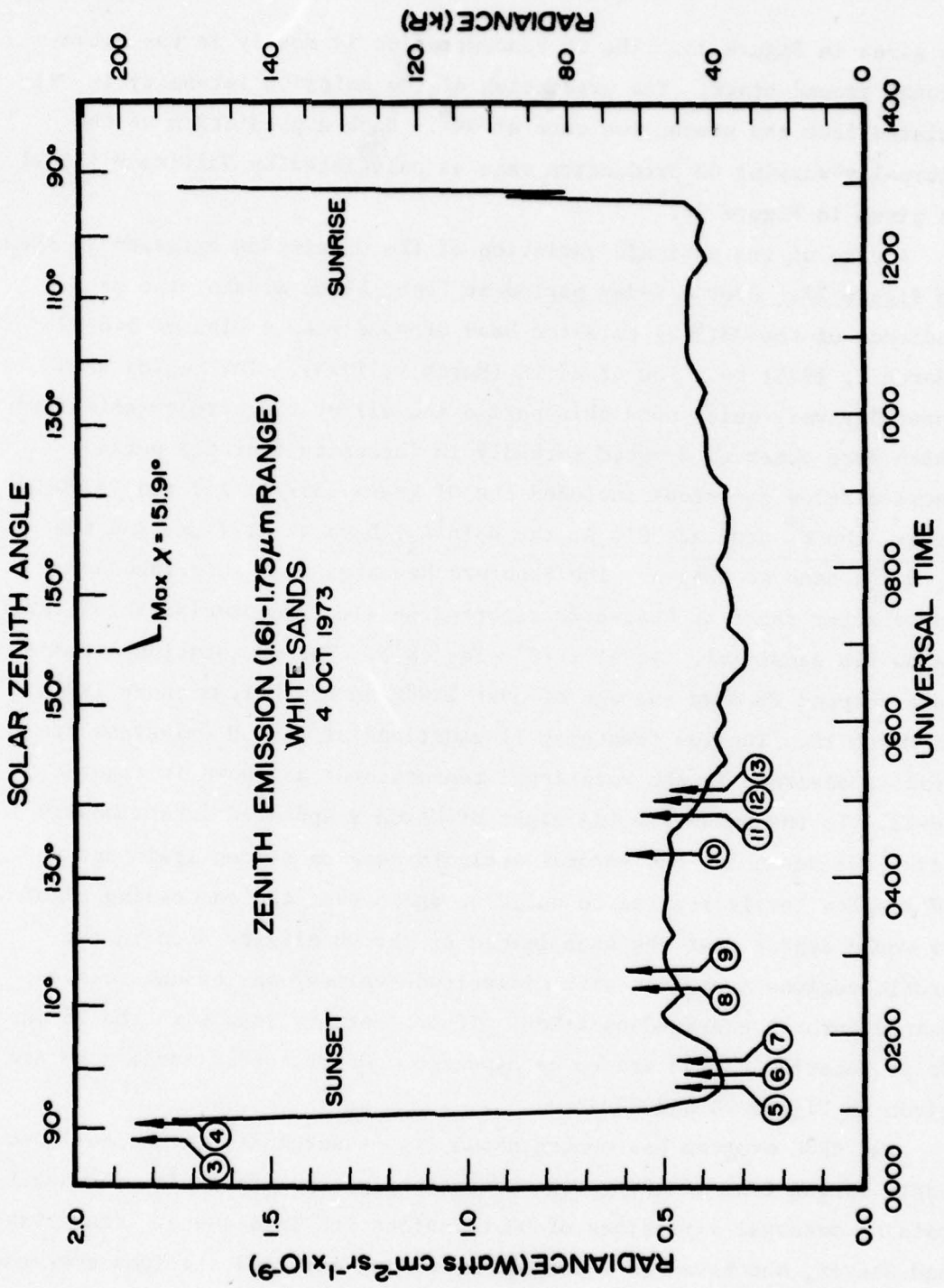

Figure 24. Zenith radiance 1.55 to 1.72 μm, White Sands on 3-4 Oct 73. (Arrows represent rocket sampling times.)

is given in Figure 25. The OH concentration is mostly in the vibrational ground state. The prediction of the emission intensity is calculated from the production rate of $OH^{\ddagger}$. Such a prediction of the diurnally-varying OH production rate as calculated by *Gattinger* [1969] is given in Figure 26.

A case of the periodic variation of the OH airglow emission is shown in Figure 27. Over a 9-day period at Poker Flat, Alaska, the zenith radiance of the OH(5,3) emission band dropped from a high of 140 kR (March 1, 1975) to a low of 20 kR (March 9, 1975). The region was aurorally very quiet over this period and all of the airglow emissions which were observed dropped markedly in intensity over the period. These airglow emissions included the OI green (5577A) and red (6300 A) lines, the N_2^+ band at 3914 A, the $O_2(a^1\Delta_g)$ band at 1.27 μm, and the $O_2(b^1\Sigma_g^+)$ band at 8645 A. The Stanford Research Institute incoherent backscatter radar at Chatanika reported an electron precipitation level below its sensitivity level ($\sim 10^5$ elec/cm^3). The OH rotational temperature dropped from an average of over 220°K on March 1, to under 190°K on March 10. The low frequency fluctuations of the OH emissions are readily apparent in the rotational temperatures as shown in Figures 20-22. To the human eye the night of March 9 appeared exceptionally dark. On March 10, the auroral activity came on strong again and the OH airglow levels started to build up again over the succeeding nights. It would appear that the high levels of the OH airglow seen in the arctic regions (compared with midlatitude values) may be due to sustained auroral energy-deposition. If so, correlations with the 28-day solar rotation period are to be expected. Other auroral-zone data are given in Figure 28 and 29.

The AFGL program has concentrated its measurements in the fall and early spring time of the year. Consequently, the statistics for ascertaining seasonal variations of OH emissions are inadequate. Krassovski and Sherof, who have led a program involving numerous stations over the Soviet Union, have the statistical base for phenomenologically assessing the changes of the OH airglow with season and from year to year over the 11-year solar cycle. The trend is for higher airglow levels in the winter than in the summer and for higher levels during periods of solar sunspot activity.

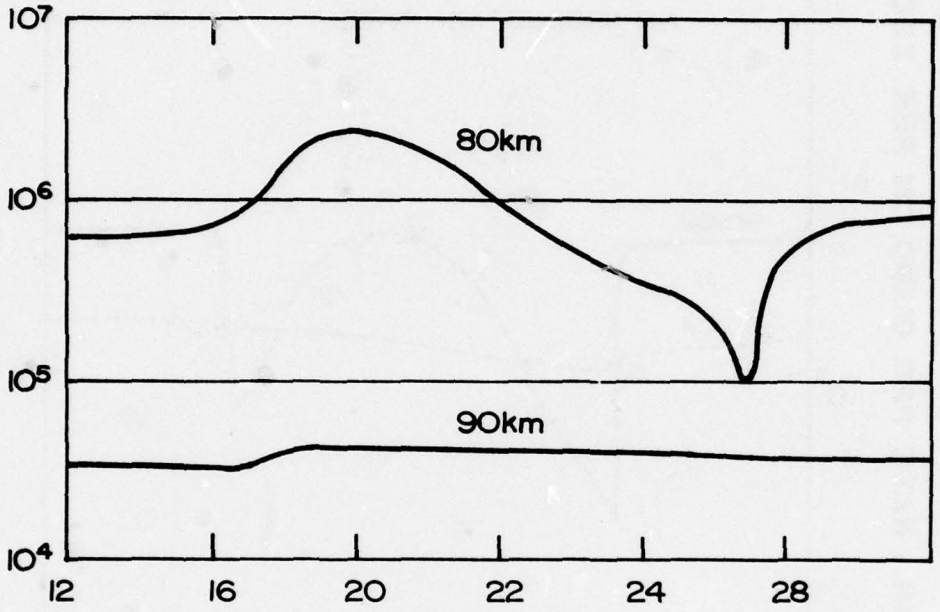

Figure 25. Diurnal variation of OH concentration predicted by *Moore and Kennealy* [1975] for early March at White Sands.

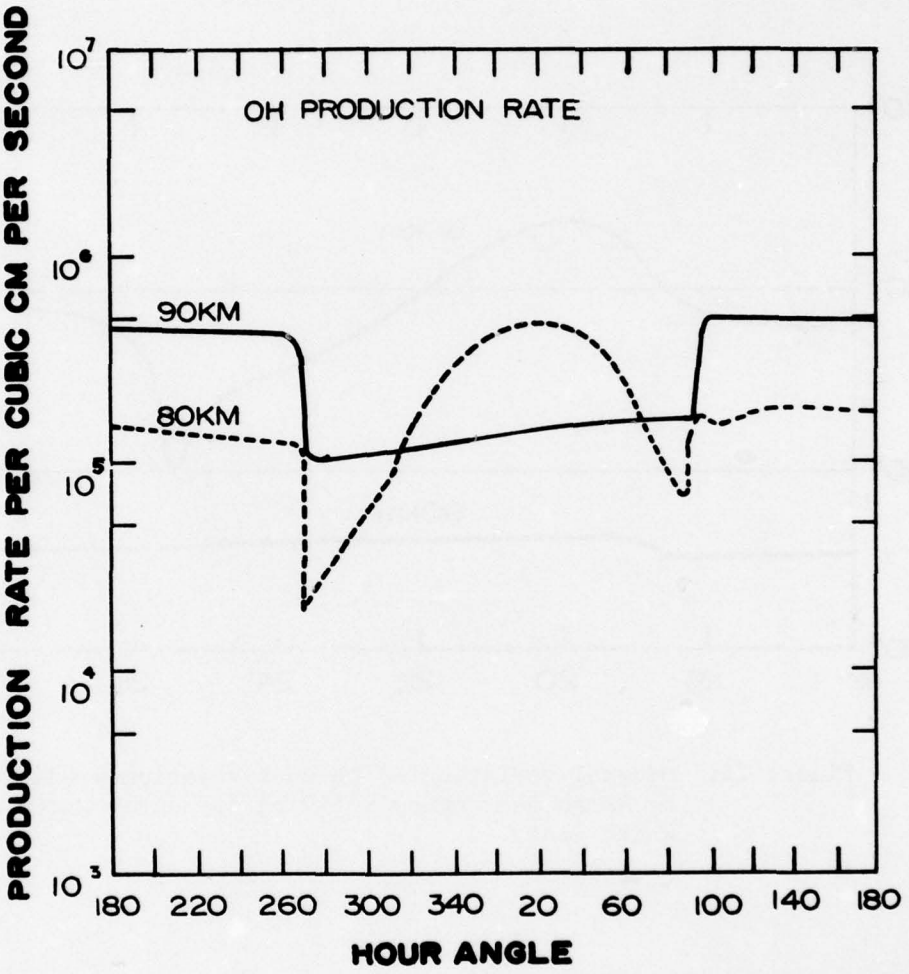

Figure 26. Theoretical prediction by *Gattinger* [1969] of diurnal variation of OH emission.

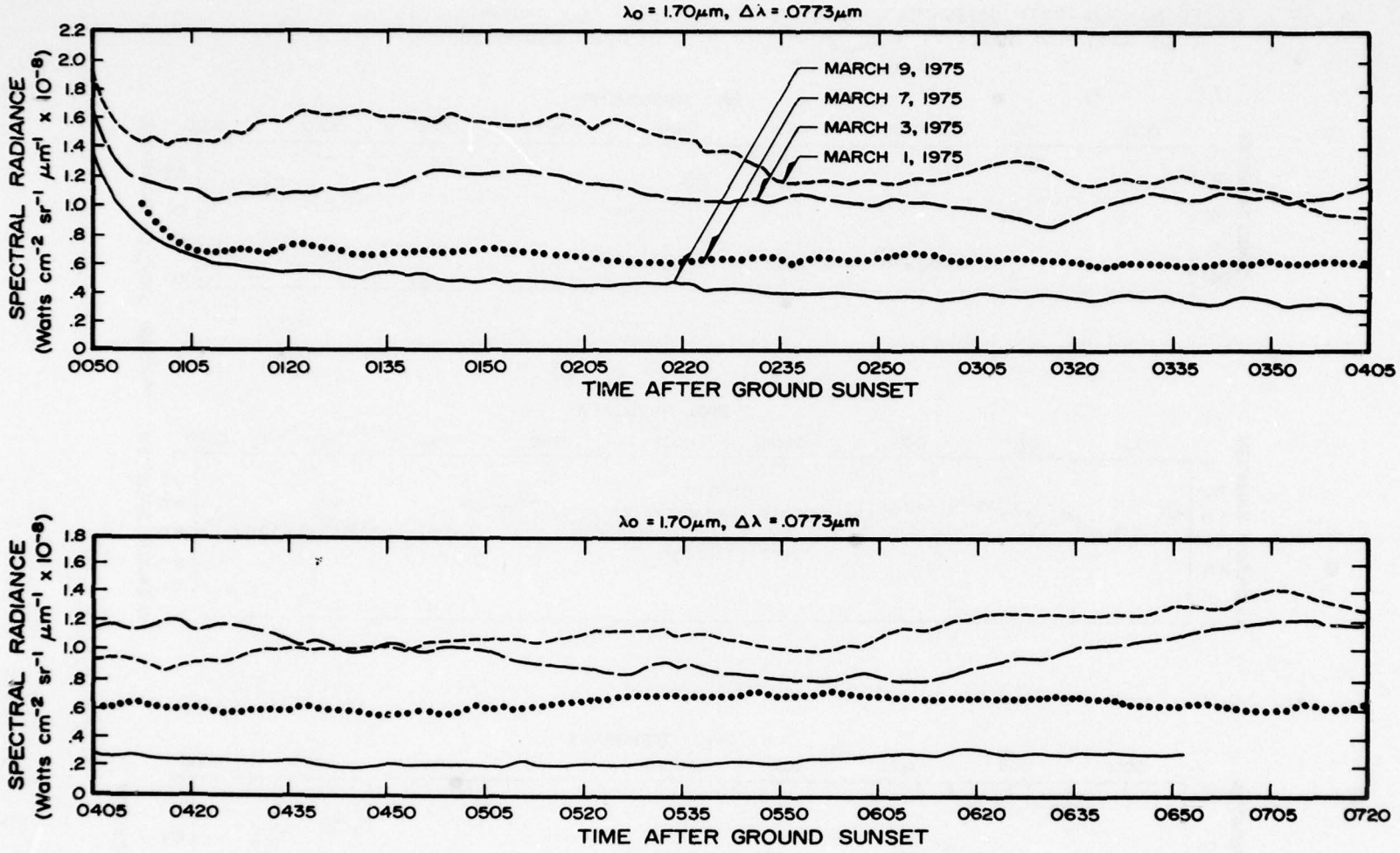

Figure 27. Pronounced intensity variations of first overtone hydroxyl (5,3) emission band over an eight day period at Poker Flat, Alaska.

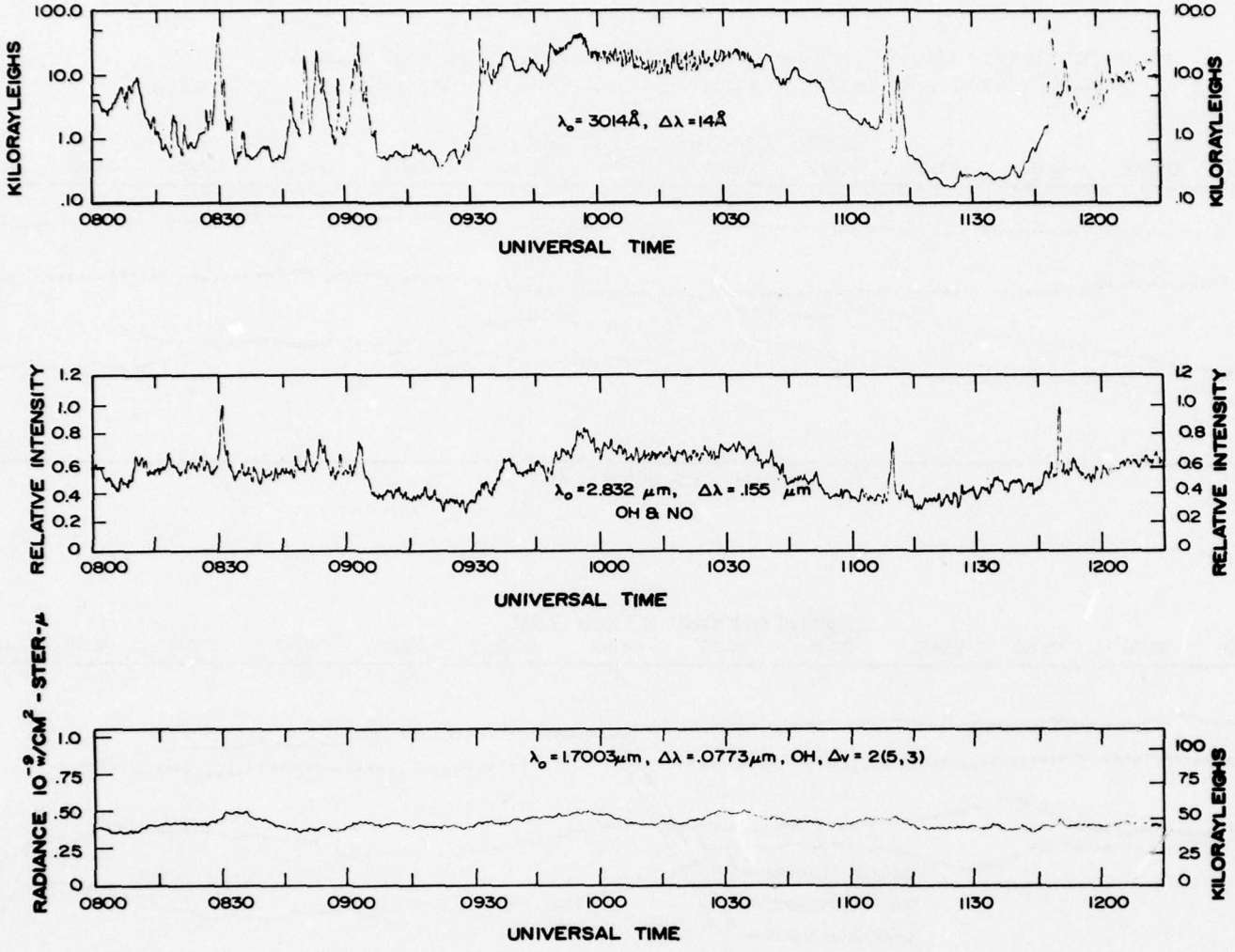

Figure 28. Measurements made by USU/AFCRL of 3914 Å, first overtone OH, fundamental OH, and NO on March 10 from the AFCRL aircraft S/N-53120.

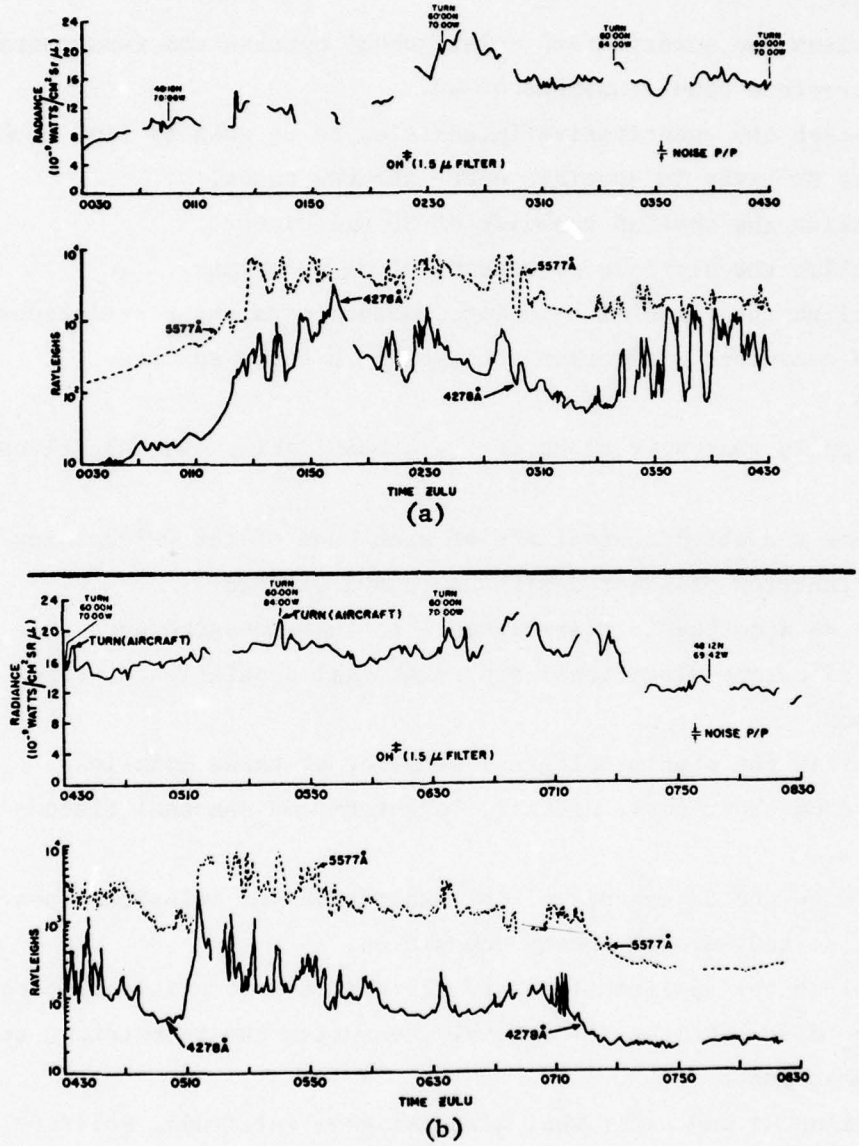

Figure 29. Visible and near infrared zenith radiance measurements taken December 12, 1968 on an aircraft flight from Boston into the auroral oval and return. (a) 0030 to 0430 hrs, (b) 0430 to 0830 hrs.

VIII. PROGRAM OBJECTIVES AND GOALS

A. Objectives

The priority objectives in satisfying the mission of the program are as follows:

1. Establish the quantitative relationship between the fundamental and overtone band sequences of OH.
2. Establish the quantitative intensities to be seen by limb looks at the OH layer in specific near-infrared bands.
3. Establish the spatial behavior of OH emissions.
4. Establish the altitude dependence of OH emissions.
5. Establish the temporal behavior, enhancements and correlations of OH emissions with other atmospheric airglow species.

B. Goals

Specific goals that need to be met in accomplishing the objectives include:

1. Measure the absolute radiance of each band of the $OH^{\ddagger}$ airglow as a function of solar zenith angle and altitude.
2. Apply an atmospheric transmittance to these measurements and then calculate vibrational and rotational population distributions.
3. Establish the phenomenological behavior of these emissions regarding short-term, diurnal, long-term and seasonal fluctuations.
4. Determine the dependency of $OH^{\ddagger}$ excitation and emissions upon latitude and auroral energy deposition.
5. Establish the applicability and reliability of rotational population distributions for remotely measuring the temperature at the mesopause.
6. Determine if and under what circumstances (altitude, solar angle, etc.) HO_2 plays a significant role in the excitation of $OH^{\ddagger}$ in the earth's upper atmosphere.
7. Determine the circumstances (altitude, solar angle, etc.) that quenching (O, O_2, etc.) plays on the level populations and therefore on the emission intensity distributions.

8. Establish the characterization and causative mechanisms for observed dynamical behavior, including apparent wavemotion and patchiness, of $OH^{\ddagger}$ airglow.
9. Determine the parameters necessary for computer codes to predict $OH^{\ddagger}$ emission means and variances for emissions within the bandpasses of both limb-look and staring sensors for the geometries which are applicable.
10. Measure the concentrations of H_2O at mesospheric altitudes.
11. Establish the temperature dependence of the reaction rates involved in OH photochemistry.
12. Establish the energy level dependence of the $OH^{\ddagger}$ quenching rates.
13. Establish strengths of long path absorption and stimulated emission effects in OH.

IX. SUMMARY OF PRESENT STATUS

A. Field Experiments

The experiments that are being planned and carried out by AFGL in accomplishment of the program mission include rocketborne, aircraft-borne and ground measurements of the OH atmospheric airglow together with related atmospheric parameters. Quantitative measurements are sought at state-of-the-art resolution with regards to: (1) spectral distributions, (2) temporal variations, and (3) three-dimensional spatial distributions.

B. Rocket Flights

A summary of the rocket flights carried out under the AFGL/USU hydroxyl measurements program is given as Table 14. In the 1965 flight a visible photometer was used to measure the OH(8,3) band [*Baker and Waddoups*, 1967]. All of the other flights employed near infrared radiometers. The filter bandpasses were discussed under Section VII-A.

Table 16. Field experiments planned or carried out which support the OH program.

Field Experiments	Assist Objectives
1. 1975 Aircraft Traverses	#1, 3, 5
2. 1976 Aircraft Traverses	#3, 5
3. 1976 FWI Rocket	#1,4
4. 1973-76 SWIR Rockets	#1, 2, 4
5. 1973-76 Ground Measurements	#3, 5
6. 1977 A/C FWI and RAD	#1, 3, 5
7. 1977-8 Satellite Measurement	#1, 2, 4

Table 17. AFGL/USU rocket flights to measure OH.

Rocket Number	Date	Time (UT)	Location*	Solar Zenith Angle (χ°)	Apogee (km)
AD3.722	Sep 25, 1965	0300	WSMR		
AD3.723	Sep 29, 1966	0249	WSMR		
A30.205-3	Mar 6, 1972	1214	PFRR	116	
A30.205-5	Mar 21, 1973	1011	PFRR	114.7	78
A30.205-6	Apr 6, 1973	0845	PFRR	107.5	78
A030.311-1	Oct 4, 1973	0040	WSMR	56	52
A030.311-2	Oct 4, 1973	0127	WSMR	99	102
A030.311-3	Oct 4, 1973	0500	WSMR	141	106
A30.311-8	Dec 2, 1975	1256	WSMR	101.4	
A30.311-5	Dec 2, 1975	1350	WSMR	90.8	
A30.311-7	Dec 2, 1975	1559	WSMR	68.7	
A30.205-7	Dec 2, 1975	0059	WSMR	102.3	
IC503.14-3	Mar 1, 1975	0100	PFRR	79.8	111
IC506.14-2	Mar 4, 1975	0739	PFRR	116	100

WSMR = White Sands Missile Range, New Mexico

PFRR = Poker Flat Research Range, Alaska

X. REFERENCES

Anderson, J.G., and T.M. Donahue, "The neutral composition of the stratosphere and mesosphere," *J. Atmos. and Terr. Physics*, 37:865-884; 1975.

Anlauf, K.G., R.G. MacDonald and J.C. Polanyi, "Infrared chemiluminescence from H^+O_3 at low pressure," *Chem. Phys. Letters*, 1:619-622; April, 1968.

Armstrong, "The influence of a gravity wave on the airglow hydroxyl rotational temperature at night," *J. Atmos. and Terr. Physics*, 37:1585-1591; 1975.

Baker, D.J., and R.O. Waddoups, "Rocket measurement of midlatitude night airglow emissions," *J. Geophys. Res.*, 72(19):4881-4883; Oct. 1, 1967.

Baker, D.J., and R.O. Waddoups, "Correction to paper by D. Baker and R. Waddoups, 'Rocket measurement of midlatitude night airglow emissions'," *J. Geophys. Res., Space Optics*, 73(7):2546-2547; 1968.

Baker, D.J., K.D. Baker, L.R. Megill and B.P. Sandford, "Infrared emission in the disturbed mesosphere and lower thermosphere," AMS Symposium in the Dynamics of the Mesosphere and Lower Atmosphere, Univ. Colorado, Boulder; June 15, 1970.

Baker, D.J., K.D. Baker, W.R. Grieder, J.C. Ulwick and A.T. Stair, Jr., "Midlatitude twilight D-region studies, White Sands, New Mexico," Utah State University and A.F. Cambridge Research Laboratories; Nov. 16, 1973.

Baker, D.J., A.J. Steed and A.T. Stair, Jr., "Ground observations of resolved hydroxyl (Δv=2) airglow," *J. Geophys. Res.*, 78(36):8859-8863; Dec. 20, 1973.

Baker, D.J. and A.T. Stair, Jr., "Hydroxyl first overtone emissions," SA-86, 1975 Fall Annual Meeting, American Geophysical Union, San Francisco; December 11, 1975. *EOS, Transactions, American Geophysical Union*, 56(12):1039; December, 1975.

Ballif, J.R., and S.V. Venkateswaram, "On the temporal variations of the OH nightglow," *J. Atmos. Sciences*, 20(1):1-57; January, 1963.

Bates, D.R., and M. Nicolet, "The photochemistry of atmospheric water vapor," *J. Geophys. Res.*, 55:301-327; 1950.

Benedict, W.S., E.K. Plyler and J.C. Humphreys, "The emissions spectrum of OH from 1.4 to 1.7 μ," *J. Chem. Phys.*, 21(3):398-402; March, 1953.

Brieg, E.L., "Secondary production processes for the hydroxyl atmospheric airglow," *Planet. Space Sci.*, 18:1271-1274; 1970.

Bunn, F.E., and H.P. Gush, "Spectrum of the airglow between 4 and 8 microns," *Can. J. Phys.*, 48:98; 1970.

Bunn, F.E., and H.P. Gush, "Spectrum of the airglow between 3 and 4 microns," *Can. J. Phys.*, 50:213; 1972.

Charters, P.E., R.G. MacDonald and J.C. Polanyi, "Formulation of vibrationally excited OH by the reaction $H+O_3$," *App. Opt.*, 10: 1747; 1971.

Connes, J., and H.P. Gush, "Spectroscopie du Ciel Nocturne dans 1'Infrarouge par Transformation de Fourier," *Le Journal de Physique et le Radium*, 20:915; 1959.

Connes, J., and H.P. Gush, "Etude du Ciel Nocturne dans the Proche Infra-rouge," *J. Phys. Radium*, 21:645; 1960.

Davis, D.D. et al., "Recent kinetic measurements on the reactions of $O(^3P)$, H and HO_2. In *Proc. 2nd Conf. on CIAP* (Ed. A.J. Broderick), U.S. Dept. of Transportation; November 14-17, 1972.

Evans, W.F.J., and E.J. Llewellyn, "Altitude distribution of hydroxyl bands of Δv=2 sequence in nightglow," *Can. J. Phys*, 51:1288; 1973.

Ferguson, A.F., and D. Parkinson, "The hydroxyl bands in the nightglow," *Planet. Space Sci.*, 11:149-159; 1963.

Gattinger, R.L., "Interpretation of airglow emissions--OH emissions," *Ann. Geophys.*, 25(4):825-830; 1969.

Good, R.E., "Determination of atomic oxygen density from rocketborne measurement of hydroxyl airglow," *Planet. Space Sci.*, 24:389-395; 1976.

Grieder, W., D.J. Baker, K.D. Baker and J.C. Ulwick, "Program Plan--Midlatitude twilight D-region studies," A.F. Cambridge Res. Labs. and Utah State University; July 21, 1973.

Grieder, W.R., K.D. Baker, A.T. Stair, Jr. and J.C. Ulwick, "Rocket measurement of OH emission profiles in the 1.56 and 1.99 μm bands," *AFCRL-TR-76-0057, Env. Res. Papers No. 550, HAES Rept. No. 38*, 73 pp. Air Force Cambridge Research Laboratories, Hanscom AFB, Mass.; January 28, 1976.

Gulledge, I.S., and D.M. Packer, "A new rocket measurement of the altitudes of OH bands in the night airglow," General assembly IUGG, IAGA-264, VII-6; 1967.

Gush, H.P., and A.V. Jones, "Infrared spectrum of the night sky from 1.0 μ to 2.0 μ," *J. Atmos. Terr. Physics*, 7:285; 1955.

Gush, H.P., and H.L. Buijs, "The near infrared spectrum of the night airglow observed from high altitude," *Can. J. Phys.*, 42:1037; 1964.

Harrison, A.W., and A.V. Jones, "Measurements of the absolute intensity of the aurora and night airglow in the 0.9 - 2.0 μ region," *J. Atmos. Terr. Physics*, 11:192; 1957.

Harrison, A.W., "Altitude profile of airglow hydroxyl emission," *Can. J. Physics*, 48:2231-2234; 1970.

Harrison, A.W., and D.J.W. Kendall, "Airglow hydroxyl intensity measurement, 0.6 - 2.3 μ," *Planet. Space Sci.*, 21:1731; 1973.

Heaps, H.S., and G. Herzberg, "Intensity distribution in the rotation-vibration spectrum of the OH molecule," Z. *Phys.*, 133:48-64; 1952.

Herzberg, G., Molecular spectra and molecular structure, *I. Spectra of Diatomic Molecules*, D. Van Nostrand Co., Princeton; 1950.

Herzberg, G., *The Spectra and Structures of Simple Free Radicals*, 49 pp., Cornell Univ. Press, Ithaca; 1971.

Hunten, D.J., "Spectroscopic studies of the twilight airglow," *Space Sci. Rev.*, 6:493-573; 1967.

Huppi, E.R., and A.T. Stair, "Sunset to sunrise variations of the OH emission of the night sky," In *Atmospheric Emission*, 471-475 pp., (Eds. B.M. McCormac and A. Omholt); 1969.

Huppi, R.J., and D.J. Baker, "Aircraft infrared measurements," *Final Report AFCRL-TR-74-0108*, 32 pp., Contract No. F19628-71-C-0059, Utah State University, Logan; January 31, 1974.

Huppi, R.J., and D.J. Baker, "Intensity variations of atmospheric hydroxyl emissions," *Scientific Report No. 1, AFCRL-TR-76-0032*, Contract No. F19628-74-C-0190, Utah State University, Logan; January 1, 1976.

Jones, A.V., and H.P. Gush, "Spectrum of the night sky in the range 1.2 - 2 μ," *Nature*, 172:496; 1953.

Kaufman, F., "Aeronomic reactions involving hydrogen, a review of recent laboratory studies," *Ann. Geophys.*, 20:106; 1964.

Kennealy, J.P., "Modeling of night-time OH production at 50 km," Unpub. Rept., Air Force Cambridge Research Labs.; 1975.

Krassovsky, V.I., "Hydroxyl emission in the upper atmosphere," *Planet. Space Sci.*, 10:7-17; 1963.

Krassovsky, V.I., "The hydroxyl emission problem and paths of its solution," *Ann. Geophys.*, 27(2):211-221; 1971.

Krassovsky, V.I., "Infrasonic variations of OH emission in upper atmosphere," *Ann. Geophys.*, 28:739; 1972.

Krassovsky, V.I., "Rotational and vibrational hydroxyl excitation in the laboratory and in the night airglow," *J. Atmos. Terr. Physics*, 35:705; 1973.

Krassovsky, V.I., and M.V. Shagae, "Optical method of recording acoustic or gravity waves in upper atmosphere," *J. Atmos. Terr. Physics*, 36(2):373; 1974.

Krassovsky, V.I., and M.V. Shagae, "Inhomogeneities and wavelike variations of rotational temperature of atmospheric hydroxyl," *Planet. Spac.*, 22(9):1334; 1974.

Krassovsky, V.I., "Ozone-hydrogen hypothesis of the hydroxyl nightairglow," *The Airglow and the Aurorae*, E.B. Armstrong ed., et al., Pergamon Press p. 197; 1956.

Kvifte, G., "Nightglow observations at Å̊s during the I.G.Y.," *Geofysiske Publikasjoner*, 20(12):14; 1959.

Kvifte, G., "Temperature measurements from OH bands," *Planet. Space Sci.*, 5:153; 1961.

Lowe, R.P., and E.A. Lytle, "Balloon-borne spectroscopic observation of the infrared hydroxyl airglow," *Appl. Opt.*, 12:579; 1973.

Lytle, E.A., and J. Hampson, "Observation of the OH dayglow," *Nature*, 202:76; 1964.

Maeda, K., "The auroral O_2-dissociation and the infrared OH-emission," Annal. Geophys., Vol. 24, No. 1, p. 173; 1968.

McDonald, R., H.L. Buijs and H.P. Gush, "Spectrum of the night airglow between 3 and 4 microns," *Can. J. Phys.*, 46:2575; 1968.

Meinel, A.B., "Hydride emission bands in the spectrum of the night sky," *Astrophys J.*, 111:207; 1950.

Meinel, A.B., "OH emission bands in the spectrum of the night sky," *Astrophys. J.*, 111:555; 1950.

Meriwether, J., "Measurements of mesosphere temperatures from intensity ratios of hydroxyl rotational components," *J. Am. Geophy.*, 55(12): 1158; 1974.

Meriwether, J.W., "High latitude airglow observations of correlated short term fluctuations in hydroxyl meinel 8-3 band intensity and rotational temperature," *Planet. Spac.*, 23(8):1211-1221; 1975.

Mies, F.H., "Calculated vibrational transition probabilities of OH($X^2\Pi$)," *J. Molecular Spectroscopy*, 53:150-188; 1974.

Moreels, G., W.F.J. Evans, J.E. Blamont and A.V. Jones, "A balloon-borne observation of the intensity variation of the OH emission in the evening twilight," *Planet. Space Sci.*, 18:637-640; 1970.

Moreels, G., A.V. Jones and J.E. Blamont, "Balloon observations of 8-6 band in day and night airglow," *Planet. Spac.*, 21:88; 1973.

Moreels, G., A.V. Jones and J.E. Blamont, "Balloon study of OH airglow emission from evening twilight to sunrise," *Can. J. Phys.*, 51:888; 1973.

Moroz, V.I., "The night-airglow infrared emission spectrum to 3.4 μ," *Astron. Zh.*, 37:123; 1960.

Murphy, R.E., "Infrared emission of OH in the fundamental and first overtone bands," *J. Chem. Phys.*, 54:4852-4859; 1971.

Nicolet, M., "Ozone and hydrogen reactions," *Ann. Geophys.*, 26:531-544; 1970.

Noxon, J.F., A.W. Harrison and A.V. Jones, "The infra-red spectrum of the night airglow from 1.4 μ to 4.0 μ," *J. Atmos. Terr. Phys.*, 16:246; 1959.

Noxon, J.F., "The latitude dependence of OH rotational temperature in the night airglow," *J. Geophys. Res.*, 69:4087; 1964.

Packer, D.M., "Altitudes of the night airglow radiations," *Ann. Geophys.*, 17:67-75; 1961.

Peterson, A.W. and L.M. Kieffaber, "Airglow fluctuations at 2.2 μ, *Ann. Geophys.*, 34:1357; 1972.

Pick, D.R., E.J. Llewellyn and A.V. Jones, "Twilight airglow measurements of the OH and O_2 bands by means of balloon-borne instruments," *Can. J. Phys.*, 49:897; 1971.

Polanyi, J.C., "Proposal for an infrared maser dependent on vibrational excitation," *J. Chem. Physics*, 34:347-348; 1961.

Potter, A.E., R.N. Colthorp and S.D. Worley, "Mean radiative lifetime of vibrationally excited (v=9) hydroxyl. Rate of reaction of vibrationally excited hydroxyl (v=9) with ozone," *J. Chem. Phys.*, 54:992; 1971.

Reed, E., "Polar enhancement of hydroxyl and continuum emissions near 6230 A," *J. Am. Geophy.*, 56(9):600; 1975.

Rogers, J.W., R.E. Murphy, A.T. Stair, Jr. and J.C. Ulwick, "Rocket-borne radiometer measurements of OH in the auroral zone," *J. Geophys. Res.*, 78:7023; 1973.

Schiff, H.I., "Excitation mechanisms for the atomic oxygen and OH emissions in the night airglow," *Bull. Soc. Chim. Belg.*, 71:670-681; 1962.

Shefov, N.N., "Hydroxyl emission of the upper atmosphere I. Behavior during a solar cycle, seasons and geomagnetic disturbances," *Planet. Space Sci.*, 17:797-813; 1969.

Shefov, N.N., "Hydroxyl emission of the upper atmosphere. II. Effects of a sunlit atmosphere," *Planet. Space Sci.*, 17:1629-1639; 1969.

Shefov, N.N., "On the correlation between the emission intensity of the O_2 atmospheric system and the vibrational temperature of the OH bands," *Astron. Circular*, U.S.S.R., Acad. Sci.; 1970.

Shefov, N.N., "Hydroxyl emission of the upper atmosphere. III. Diurnal variations," *Planet. Space Sci.*, 18:129-136; 1971.

Shemansky, D.E., and A.V. Jones, "New measurements of the night airglow spectrum in the 1.5 μ region," *J. Atmos. Terr. Phys.* 22:166; 1961.

Sivjee, G.G., "Spectro-photometry of the night airglow and the aurorae," *Ph D Dissertation*, John Hopkins Univ., Baltimore; 1970.

Streit, G.E., and H.S. Johnston, "Reactions and quenching of vibrationally excited hydroxyl radicals," *J. of Chem. Phys.*, 64(1); January 1, 1976.

Stair, A.T., Jr., J.P. Kennealy and S.P. Stewart, Jr., "Observation of the v = 1 sequence of OH produced in the H^+O_2 Reaction," *Planet. Space Sci.*, 13:1005; 1965.

Stair, A.T., *et al.*, "Auroral region enhancement of OH emission," *The Radiating Atmosphere*, Dordrect, Holland; 1970.

Stair, A.T., Jr., and D.J. Baker, "Midlatitude hydroxyl IR airglow spectra," AFCRL-TR-74, Air Force Cambridge Res. Lab., L.G. Hanscom Field, Bedford, Mass., 172 pp.; February 1, 1974.

Stair, A.T. Jr., and D.J. Baker, "Auroral zone hydroxyl infrared spectra," AFCRL-TR-74, Air Force Cambridge Res. Labs., L.G. Hanscom Field, Bedford, Mass., 366 pp.; March 1, 1974.

Steed, A.J., R.J. Huppi, R.H. Haycock and D.J. Baker, "Airborne airglow studies," *Final Report AFCRL-70-066*, Contract No. F19628-67-C-0399, Utah State University, Logan; October 31, 1970.

Ulwick, J.C., and W.F. Grieder, "Rocket measurements of OH emission profiles," Unpub. Rept., A.F. Cambridge Res. Labs., Bedford, and Utah State University, Logan, 6 pp.; 1976.

Waddoups, R.O., and D.J. Baker, "Night airglow OI green, continuum and hydroxyl emissions," *Scientific Rept. No. 5, AFCRL-68-0330*, Contract No. AF19(628)-5916, Electro-Dynamics Labs., Utah State University, Logan; June 1, 1968.

Ware, G.A., and D.J. Baker, "OH rotational temperatures at auroral latitudes," 57th Annual Meeting, American Geophysical Union, Washington, D.C. April, 1976. *EOS, Transactions, American Geophysical Union*, 57(4); April, 1976.

Warneck, P., "OH production rates in the troposphere," *Planet. Space Sci.*, 23:1507-1518; November, 1975.

Worley, S.D., R.N. Colthorpe and A.E. Potter, Jr., "Quenching of vibrationally excited hydroxyl (v=9) with oxygen," *J. Chem. Phys.*, 55:2608-2609; 1971.

Worley, S.D., R.N. Colthorpe and A.E. Potter, Jr., "Rates of interaction of vibrationally excited hydroxyl with diatomic and small polyatomic molecules," *J. Phys. Chem.*, 76(11):1511-1514; 1972.

XI. DISTRIBUTION LIST

DEPARTMENT OF DEFENSE

Director
Defense Advanced Rsch. Proj. Agency
Attn: LTC W.A. Whitaker

Defense Documentation Center
Attn: TC (2 Copies)

Director
Defense Nuclear Agency
Attn: TITL Tech. Library (3 Copies)
Attn: TISI Archives
Attn: RAEV Harold C. Fitz, Jr.
Attn: RAAE Maj. J. Mayo
Attn: RAAE G. Soper
Attn: RAAE Maj. R. Bigoni

Dir. of Defense Rsch. & Engineering
Department of Defense
Attn: DD/S&SS(OS) Daniel Brockway

Commander
Field Command
Defense Nuclear Agency
Attn: FCPR

Chief Livermore Division
FLD Command DNA
Attn: FCPRL

DEPARTMENT OF THE ARMY

Commander/Director
Atmospheric Sciences Laboratory
U.S. Army Electronics Command
Attn: DRSEL-BL-SY-A.F. Niles
Attn: H. Ballard

Commander
Harry Diamond Laboratories
Attn: DRXDO-NP, F.H. Wiminetz
(2 copies)

Commander
U.S. Army Nuclear Agency
Attn: Mona-We

Director
BMD Advanced Technical Center
Attn: ATC-T, M. Capps
Attn: ATC-O, W. Davies

Dep. Chief of Staff for Rsch,
Dev & Acout.
Department of the Army
Attn: MCB Division
Attn: DAMA-CSZ-C
Attn: DAMA-WSZC

Director
U.S. Army Ballistic Rsch Labs.
Attn: John Mester
Attn: Tech. Library

Commander
U.S. Army Electronics Command
Attn: Inst. for Expl. Research
Attn: Weapons Effects Section

Commander
CORADCOM
Attn: PP-Library

DEPARTMENT OF THE NAVY

Commander
Naval Oceans Systems Center
Attn: Code 2200 William Moler

Director
Naval Research Laboratory
Attn: Code 7712 D.P. McNut
Attn: Code 6701 J.D. Brown
Attn: Code 2600 Tech. Library
Attn: Code 7175J C.Y. Johnson
Attn: Code 6700 T.P. Coffey
Attn: Code 7709 Wahab Ali
Attn: Code 6780 D.F. Strobel
Attn: Code 6780 P. Juluenne
Attn: Code 67800 J. Fedder
Attn: Code 6780 S. Ossakow
Attn: Code 6707 J. Davis

Commander
Naval Surface Weapons Center
Attn: Code WA 501 Navy NUC Prgms. Off.
Attn: Technical Library

Superintendent
Naval Post Graduate School
Attn: Rech Rpts Librarian

Commander
Naval Intelligence Support Ctr
Attn: Document Control

DEPARTMENT OF THE AIR FORCE

AF Geophysics Laboratory, AFSC
Attn: LKB, K.S.W. Champion
Attn: OPR, A.T. Stair, Jr.
Attn: OPR, P.G. Doyle
Attn: OPR, R. Murphy
Attn: LKO, R. Huffman

AF Weapons Laboratory, AFSC
Attn: Maj. Gary Ganong, DES

Commander
ASD
Attn: ASD-YH-EX-LTC R. Leverette

SAMSO/AW
Attn: SZJ Lt. Col. Doan

SAMSO/YN
Attn: Maj. P. Sivgals

AFTAC
Attn: Tech Library
Attn: TD

HQ
Air Force Systems Command
Attn: DLS
Attn: Tech Library
Attn: DLCAE
Attn: DLTW
Attn: DLXP
Attn: SDR
Attn: RDQ

US ENERGY RSCH. and DEV. ADMIN.

Division of Military Application
U.S. Energy Rsch & Dev Admin
Attn: Doc. Con.

Los Alamos Scientific Laboratory
Attn: DOC CON for H.V. Argo
Attn: DOC CON for M.B. Pongratz
Attn: DOC CON for R. Brownlee
Attn: Group AP-4, MS 567
Attn: DOC CON for J. Zinn

University of California
Los Alamos Scientific Laboratory
Attn: Librarian MS 362

Sandia Laboratories
Attn: DOC CON for W.B. Brown, Org. 1353
Attn: Tech. Library, Org. 3141

Argonne National Laboratory
Records Control
Attn: Doc. Con. for D.W. Green
Attn: Doc. Con. for LIR SVCS Rpts Sec
Attn: Doc. Con. for G.T. Reedy

University of California
Lawrence Livermore Laboratory
Attn: W.H. Duewer, L-262
Attn: J. Chang, L-71

U.S. Energy Rsch & Dev. Admin
Division of Headquarters Services,
Library Branch
Attn: Doc. Con. for Class. Tech. Lib.

OTHER GOVERNMENT

Department of Transportation
Office of the Secretary
Attn: S.C. Coroniti

NASA
Goddard Space Flight Center
Attn: Code 6801 A. Temkin
Attn: Tech. Library
Attn: Code 900 J. Siry

NASA
Langley Station
Attn: Tech. Library

NASA
Ames Research Center
Attn: N-245-3 R. Whitten

Department of the Army
Bal. Miss. Def. Adv. Tech. Ctr.
Attn: W.O. Davies

Federal Aviation Administration
Attn: HAPP/AEQ-10/James W. Rogers

Central Intelligence Agency
Attn: ED/SI RM 5G48 HQ Bldg.
Attn: NED/OS I-2G4R HQS

Department of Commerce
National Bureau of Standards
Attn: Sec. Officer for M. Krauss
Attn: Sec. Officer for
L.H. Gevantman

National Oceanic & Atmospheric Admin.
Environmental Research Laboratories
Department of Commerce
Attn: G. Reid
Attn: E. Ferguson
Attn: F. Fehsenfeld

DEPARTMENT OF DEFENSE
CONTRACTORS

Science Applications Inc.
Attn: D.G. Hopper

Aero-Chem Research Laboratories, Inc.
Attn: A. Fontijn
Attn: H. Pergament

Aerodyne Research, Inc.
Attn: F. Bien
Attn: M. Camac

Aerospace Corporation
Attn: N. Cohen
Attn: H. Mayer
Attn: R.J. McNeal
Attn: T.D. Taylor
Attn: J. Reinheimer
Attn: R.D. Rawcliffe

AVCO-Everett Research Laboratory
Inc.
Attn: Tech. Library
Attn: C.W. Von Rosenberg, Jr.

Battelle Memorial Institute
Attn: H.L. LaMuth
Attn: STOIAC

Brown Engineering Company, Inc.
Attn: N. Passino

General Research Corporation
Attn: D. Jones

California at Riverside, University of
Attn: J.N. Pitts, Jr.

California at San Diego, University of
Attn: S.C. Lin

California University of Berkeley
Attn: Sec. Officer for H.
Johnston
Attn: Sec. Officer for Dept. of
Chem., H.L. Strauss

Calspan Corporation
Attn: C.E. Treanor
Attn: J.M. Grace
Attn: M.G. Dunn
Attn: W. Wurster

University of Colorado
Astro-Geophysics
Attn: J.B. Pearce

Colorado, University of
Office of Contracts and Grants
Attn: G.M. Lawrence, LASP

Concord Sciences
Attn: E.A. Sutton

University of Denver
Space Science Laboratory
Attn: B. Van Zyl

University of Denver
Denver Research Laboratory
Attn: Sec. Officer for D.
Murcray

General Electric Company
Tempo-Center for Advanced Studies
Attn: DASAIC
Attn: W.S. Knapp
Attn: T. Stephens
Attn: D. Chandler
Attn: V.R. Strull

General Electric Company
Space Division
Attn: M.H. Bortner, Space Science Lab
Attn: J. Burns
Attn: F. Alyea
Attn: P. Zavitsands
Attn: R.H. Edsall
Attn: T. Baurer

General Research Corporation
Attn: J. Ise, Jr.

Geophysical Institute
University of Alaska
Attn: J.S. Wagner
Attn: N. Brown

Lowell University of
Center for Atmospheric Research
Attn: G.T. Best

Lockheed Missiles and Space Company
Attn: J. Kumer, Dept. 52-54
Attn: J.B. Cladis, Dept. 52-12, B202
Attn: B.M. McCormac, Dept. 52-54
Attn: T. James, Dept. 52-54
Attn: M. Walt, Dept. 52-10
Attn: R.D. Sears, Dept. 52-54

Institute for Defense Analysis
Attn: E. Bauer
Attn: H. Wolfhard

Mission Research Corporation
Attn: D. Archer
Attn: D. Fischer
Attn: M. Scheibe
Attn: D. Sappenfield
Attn: D. Sowle

Photometrics, Inc.
Attn: I.L. Kofsky

Berkeley Research Associates
Attn: J.B. Workman

Physical Dynamics Inc.
Attn: A. Thompson

Physical Sciences, Inc.
Attn: K. Wray
Attn: R.L. Taylor
Attn: G. Caledonia

Physics International Company
Attn: Doc Con for Tech Library

Pittsburgh, University of the
Comwlth
System of Higher Education
Attn: W.L. Fite
Attn: M.A. Biondi
Attn: F. Kaufman

R & D Associates
Attn: R. Latter
Attn: R.G. Lindgren
Attn: B. Gabbard
Attn: R. Lelevier
Attn: A.L. Latter
Attn: F. Gilmore
Attn: H.J. Mitchell

Rand Corporation
Attn: C. Crain

Science Applications, Inc.
Attn: D.A. Hamlin
Attn: D. Sachs

Stanford Research Institute
International
Attn: M. Baron
Attn: W.G. Chesnut

Technology International Corporation
Attn: W.P. Boquist

United Technologies Corporation
Attn: H. Michels
Attn: R.H. Bullis

Utah State University
Attn: D. Baker
Attn: K. Baker
Attn: C. Wyatt
Attn: A. Steed

Visidyne, Inc.
Attn: H. Smith
Attn: J.W. Carpenter
Attn: T.C. Degges
Attn: C. Humphrey

Wayne State University
Attn: R.H. Kummler
Attn: W.E. Kaupplia

Commander
Rome Air Development Center
Attn: OSCA, J.J. Simons

Stewart Radiance Laboratory
Attn: R. Huppi

Boston College
Space Data Analysis Laboratory
Attn: E.R. Hegblom
Attn: W.F. Grieder

Forrestial Campus Library
Princeton University
Attn: Librarian